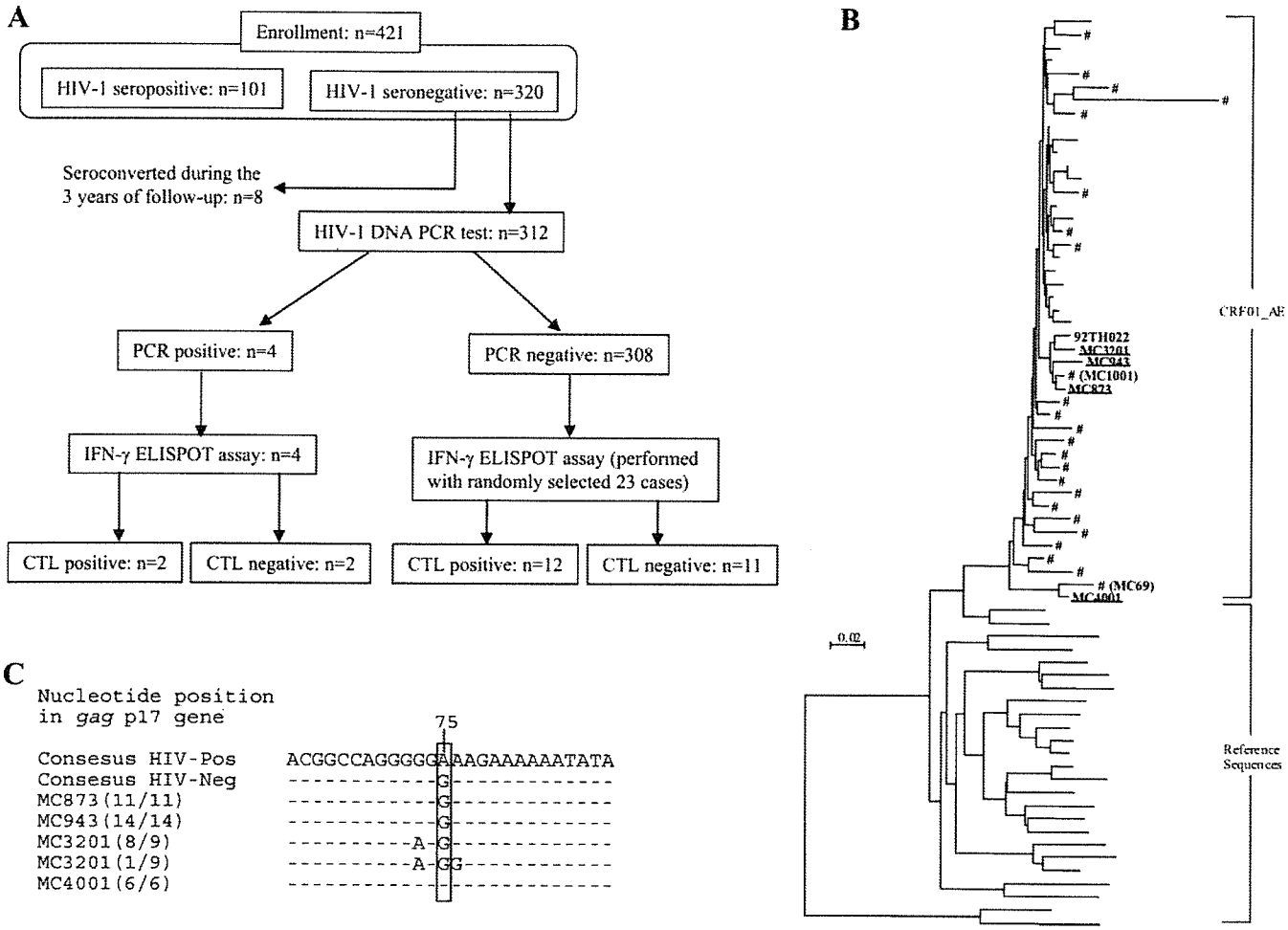

FIG. 1. Results of initial screening and phylogenetic analysis of the HIV-1 *gag* p17 gene. (A) Schematic diagram of this study. Serological studies were carried out with 421 DUs in Chiang Rai, Thailand. HIV-1 DNA PCR analysis was performed with 312 patients who were subsequently followed and who remained seronegative. The human gamma interferon enzyme-linked immunospot assay (IFN-γ ELISPOT) was performed with four seronegative but HIV-1 *gag* gene-positive DU cases and 23 randomly selected seronegative HIV-1 *gag* gene-negative DU cases to determine the anti-HIV-1 cytotoxic T-lymphocyte (CTL) responses. (B) Phylogenetic tree of the *gag* p17 gene. The neighbor-joining method was applied to obtain a phylogenetic tree with nucleotide sequences from HIV-1-seronegative but *gag* gene-positive DUs (underlined) and seropositive DUs infected with CRF01_AE in the same cohort (7) (indicated by #) together with the reference sequences from the Los Alamos National Laboratory HIV, including representatives of all group M clades and CRF01_AE (database available at http://www.hiv.lanl.gov/content/index).The infectious molecular clone G5 was constructed from isolate 92TH022 (11; Codon Usage Database at http://kazusa.or.jp/codon/; GenBank release 151.0) that was obtained in northern Thailand. (C) Sequence alignment of the *gag* p17 gene segment surrounding the nucleotide position 75 (+426). The consensus HIV-1 *gag* p17 sequences of seronegative and seropositive DU cases in the same cohort (Los Alamos National Laboratory HIV database) were obtained from the sequence comparison. The deterministic nucleotide sequence that distinguishes seronegative and seropositive cases was found at nucleotide position 75 (+426) of the *gag* p17 gene (boxed). Pos, seropositive; Neg, seronegative.

plicor HIV-1 Monitor, version 1.5; Roche Diagnostics), and the cells transfected with the clones were assayed for Gag protein expression by Western blotting (24) and transmission electron microscopy (25). Data were analyzed by the StatView program (SAS Institute, Cary, NC). A P value of < 0.05 was considered significant.

Whereas most of the samples (308 cases) were negative for HIV-1 DNA by PCR, we identified four cases (MC873, MC943, MC3201, and MC4001) positive for the HIV-1 *gag* p17 gene (Fig. 1A). Although these four cases appeared healthy without any detectable HIV-1 antigens, antibodies, viral load, or reduction of $CD4^+$ T lymphocytes, two of these four cases were found repeatedly positive for anti-HIV-1 cytotoxic T-lymphocyte responses. These four cases were followed up until November 2003, and no seroconversion was detected (data not shown).

The DNA fragment containing the *gag* p17 gene from these seronegative cases was amplified, cloned, and sequenced for further analyses. We found that the nucleotide sequences obtained from the above-mentioned four seronegative DU cases appeared to belong to the same group of CRF01_AE reference strains (Fig. 1B), suggesting their possible exposure to CRF01_AE which is prevalent in northern Thailand (Los Alamos National Laboratory HIV database available at http://www.hiv.lanl.gov/content/index).We found that the sequences of three out of four seronegative cases conform a tight cluster together with MC1001, obtained from a seropositive DU in our cohort (7), and 92TH022. MC4001 conformed to an isolated

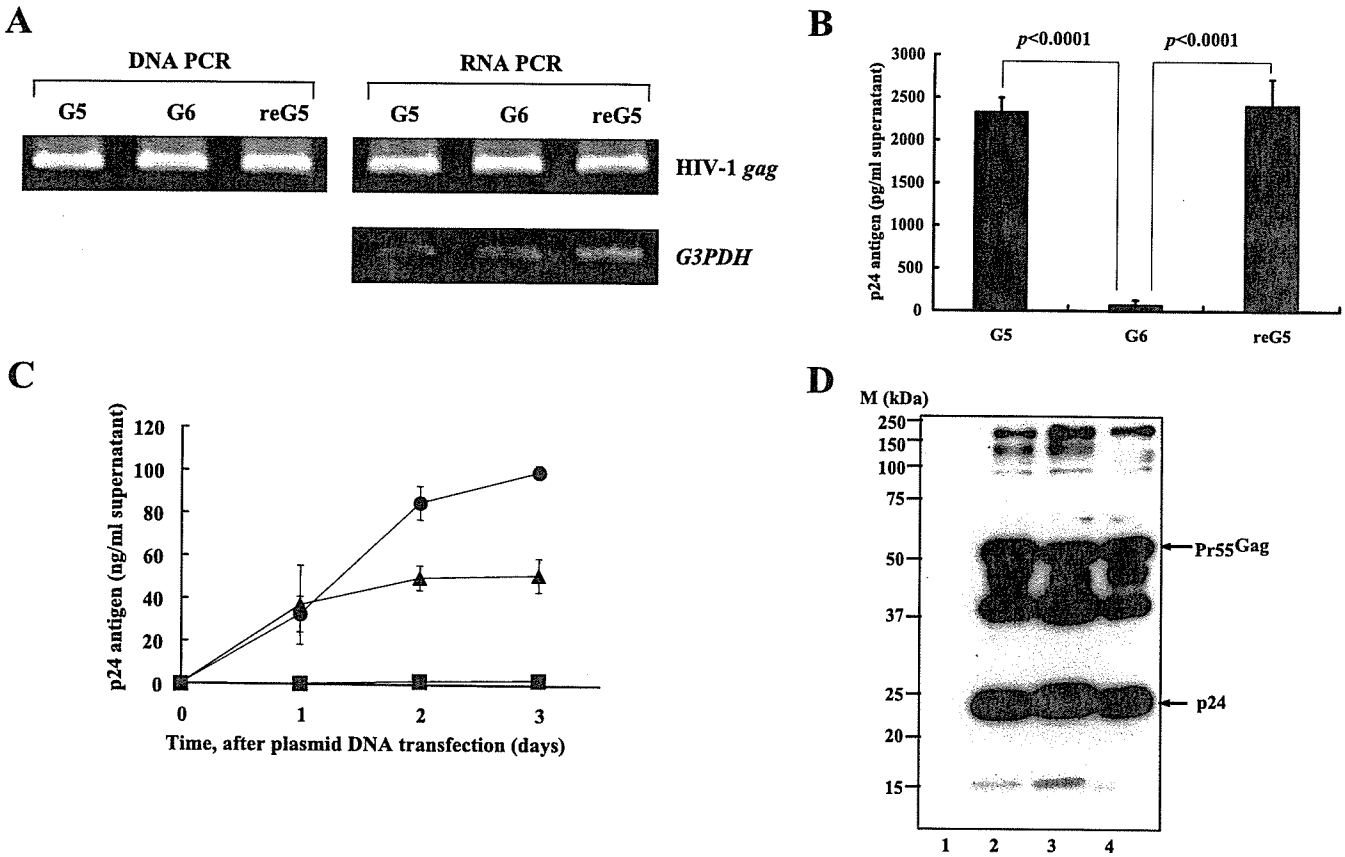

FIG. 2. Viral mRNA expression, viral protein synthesis, and virion production of G5 and G6 HIV-1 clones. (A) Detection of HIV-1 DNA and viral mRNA in cells transfected with the G5, G6 and reG5 clones. HIV-1 DNA and mRNA were detected by DNA PCR and reverse transcription-PCR (RT-PCR) with specific primers previously described (15). *G3PDH* (glyceraldehyde 3-phosphate dehydrogenase) was amplified as an internal control for RT-PCR. (B) Amounts of HIV-1 p24 antigen in the culture supernatants of cells transfected with replication-competent HIV-1 clones G5, G6, and 93JP-NH1 (12). At 24 h posttransfection, culture supernatants were subjected to the HIV-1 p24 antigen ELISA. The experiments were performed in triplicates, and the means ± standard deviations are indicated. The statistical significance was evaluated by a Student's *t* test. (C) Time course of HIV-1 virion production in the culture supernatants of transfected cells. Amounts of HIV-1 p24 antigen in the culture supernatants of cells transfected with replication-competent HIV-1 clones G5 (circle), G6 (square), and 93JP-NH1 (triangle) were measured 1, 2 and 3 days posttransfection. The experiments were performed in triplicates, and the means ± standard deviations are indicated. (D) Western blot detection of viral proteins produced in cells 48 h after transfection with replication-competent HIV-1 clones. Lane 1, negative control (vector plasmid); lane 2, G5; lane 3, G6; lane 4, 93JP-NH1 (positive control). The positions of viral $Pr55^{Gag}$ and p24 are indicated on the right. The positions of protein markers are indicated on the left.

cluster together with MC69, a seropositive DU and long-term nonprogressors living in the same village. To clarify the cause of lack of seroconversion in these DU cases, we inspected the genetic differences between HIV-1 sequences of seropositives and seronegatives in the same local cohort. Whereas the nucleotide at *gag* p17 position 75 (+426) is A in sequences of seropositives, it is G in sequences of seronegatives (Fig. 1C). Moreover, we were not able to find other conserved mutation positions between these four sequences.

We then explored the biological effect of A426G change by creating full-length HIV-1 molecular clones containing A (G5) or G (G6) at nucleotide position +426, based on the parental molecular clone 92TH022 (9,722 bp). Moreover, we also constructed a revertant mutant (reG5) in which the G substitution (G6) was reversed to an A mutation. We detected HIV-1 DNA and similar levels of viral mRNA expression in the transfected cells with the G5, G6, and reG5 clones (Fig. 2A). However, a profound reduction of HIV-1 virion production in the culture supernatant from cells transfected with G6 was observed (Fig. 2B). This also indicates that no undetected mutation was introduced during the construction of the G6 mutant clone. Furthermore, no significant increase in virus production was observed with G6 even after a prolonged period posttransfection, whereas the level of G5 virus production was comparable with that of the parental clone, 93JP-NH1 (Fig. 2C) (12). The levels of intracellular viral protein production as assayed by Western blotting and their stabilities were almost similar in clones G5, G6, and 93JP-NH1 (Fig. 2D), suggesting that the effect of a single synonymous nucleotide substitution at position +426 is not at the level of viral protein synthesis. These experiments were carried out independently in two different laboratories, and essentially the same results were obtained. These findings suggest that the major effect of the A426G nucleotide change might be at the step between viral protein synthesis and virus budding.

Abundant virion production was observed in G5-transfected cells using transmission electron microscopy (Fig. 3A). In contrast, few viral particles were detected in G6-transfected cells

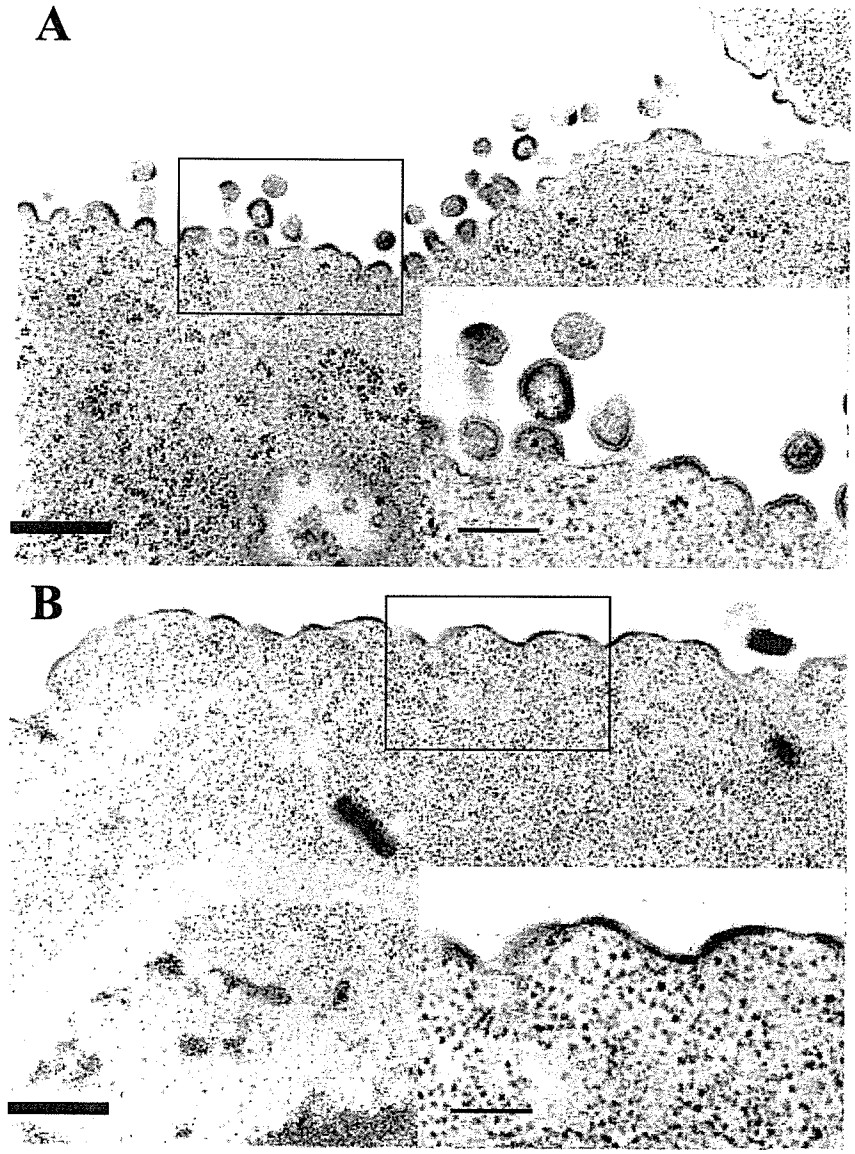

FIG. 3. Transmission electron microscopic examinations of cells transfected with G5 (A) and G6 (B). Note that mature and immature virions were observed in the cell surface of G5-transfected cells, whereas few viral particles were observed in G6-transfected cells. Higher magnifications of the boxes areas are shown as insets. Thick and thin scale bars indicate 0.5 μm and 0.2 μm, respectively.

(Fig. 3B). Although the typical dense patch structure, suggesting the accumulation of viral proteins, was observed, further viral morphogenesis appeared to be blocked in the image shown in Fig. 3B. It is also noted that the curvature of the viral-associated dense patch in the cytoplasmic membrane surface of G6-transfected cells was distinguishable from that of the G5-transfected cells: whereas the former was relatively smooth with less accumulation of high-density material, the latter was characterized by the presence of a rougher surface with more protrusions, eventually leading to virus budding, which suggests that virion morphogenesis was blocked in the membrane-associated area at the early phase of morphogenesis in G6-transfected cells. These findings suggest that a single nucleotide in the *gag* p17 gene (nucleotide position +426) may be involved in viral morphogenesis.

To further clarify the effect of the A426G mutation, we have examined the presence of viral RNA in the culture supernatant. Although viral protein and mRNA expression levels within the cells transfected with G5, G6, and 93JP-NH1 were almost equivalent (Fig. 2A and 4A), virus production in G6 was extremely low. Moreover, in parallel with the reduced virion production, significantly lower copy numbers of viral RNA were found in the supernatant (Fig. 4C). These findings clearly indicate that the A426G mutation in HIV-1 causes a serious defect in virion production.

Our data indicate that a one-nucleotide mutation in *gag* p17 without changing the amino acid is responsible for reduced HIV-1 virion production. Since viral RNA was detected in the supernatant of G6-transfected cells, though to a much lower level, this one-point synonymous mutation cannot completely abolish virus replication. This mutation is clearly different from the one described by Cannon et al. (4), who demonstrated that

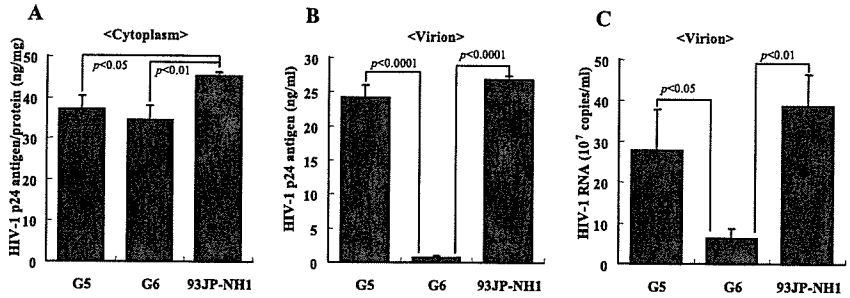

FIG. 4. Comparison of viral p24 (Gag) proteins and virion-associated viral RNA among G5, G6, and 93JP-NH1 clones. (A) Amounts of HIV-1 p24 (Gag) proteins in cells transfected with G5, G6, and 93JP-NH1 viruses. At 24 h posttransfection, whole-cell extracts were prepared and subjected to HIV-1 p24 antigen ELISA. (B) Amounts of virion-associated HIV-1 p24 in the supernatants of cells transfected with G5, G6, and 93JP-NH1 viruses. At 24 h posttransfection, cell culture supernatants were collected, and HIV-1 p24 antigen levels were determined. (C) Amounts of HIV-1 viral RNA in the supernatants of cells transfected with G5, G6, and 93JP-NH1 viruses. At 48 h posttransfection, culture supernatants were collected, and the viral RNA copy numbers were determined by an Amplicor HIV-1 Monitor (version 1.5). In these experiments, 293 cells were transfected with replication-competent full-length HIV-1 clones, G5, G6, or 93JP-NH1 (positive control), and the cells or culture supernatants were collected at indicated time points. All measurements were performed in triplicates, and the means ± standard deviations are indicated.

an amino acid mutation in the *gag* p17 coding sequence resulted in a defect in viral replication.

Findings from electron microscopic examination (Fig. 3) suggested that the G6 virus production was blocked at a step from virion assembly through virus budding in spite of the presence of thick, patchy densities in the cytoplasmic membrane that are indicative of the tethering of viral proteins. Thus, the reduced virion production may be due to diminished protein accumulation to the lipid raft formed at the inner face of the host cell plasma membrane.

HIV-1 virion assembly is initiated by the plasma membrane translocation of $Pr55^{Gag}$ and $Pr160^{Gag\text{-}Pol}$ (6). Formation of virus-like particles by $Pr55^{Gag}$ is a self-assembly process with critical Gag-Gag interactions between multiple domains along Gag precursor, and the assembly of virus-like particles does not necessarily require the participation of viral genomic RNA (1). The interaction between $Pr55^{Gag}$ and viral genomic RNA, as well as dimerization of viral genomic RNA, is considered crucial for HIV-1 morphogenesis (17). However, in spite of our repeated trials, an RNA-protein interaction between the HIV-1 packaging sequence spanning +223/+506 containing A426 (G5) or G426 (G6) and HIV-1 nucleocapsid did not show any difference between G5 and G6 sequences, at least in vitro (data not shown). It is possible that a subtle mutation like A426G may not cause a robust loss in the affinity to the nucleocapsid in the absence of a milieu of cellular and viral proteins. Roldan et al. (18) reported that the viral RNA segment spanning the region +400 to +500, containing A426, is involved in the binding to $Pr55^{Gag}$ and acts as a major packaging sequence, which may explain our finding that the nucleotide A426 in the *gag* p17 gene is crucial for the virion production.

Collectively, although the nucleotide substitution of A to G at position +426 of the *gag* p17 gene appears to contribute to reduced levels of virus production, further studies are crucial to understand the underlying mechanism. These studies should not only decipher a novel regulatory mechanism of viral production but might also indicate a possible target for novel HIV-1 therapy.

We gratefully acknowledge the dedicated field work of S. Moolphate, P. Saksoong, and other members of the TB/HIV Research Project, the RIT-JATA, the Regional Medical Sciences Centre in Chiang Rai, and the Mae Chan Hospital. The technical assistance of S. Sapsutthipas and J. Phromjai is very much appreciated. We thank H. Sato for kindly supplying the infectious molecular clone, 93JP-NH1. We also thank K. Balachandra, M. Honda, T. Nakasone, and Y. Takebe for kind technical support and advice.

This work was supported by grants-in-aid from the Ministry of Health, Labor and Welfare, Japan; Ministry of Education, Culture, Sports, Science and Technology, Japan; the Sasakawa Memorial Health Foundation; the Japanese Foundation for AIDS Prevention; and the Japan Health Sciences Foundation.

REFERENCES

1. **Bennett, R. P., T. D. Nelle, and J. W. Wills.** 1993. Functional chimeras of the Rous sarcoma virus and human immunodeficiency virus gag proteins. J. Virol. **67**:6487–6498.
2. **Beretta, A., S. H. Weiss, G. Rappocciolo, R. Mayur, C. De Santis, J. Quirinale, A. Cosma, P. Robbioni, G. M. Shearer, J. A. Berzofsky, M. L. Villa, A. G. Siccardi, and M. Clerici.** 1996. Human immunodeficiency virus type 1 (HIV-1)-seronegative injection drug users at risk for HIV exposure have antibodies to HLA class I antigens and T cells specific for HIV envelope. J. Infect. Dis. **173**:472–476.
3. **Bryson, Y. J., S. Pang, L. S. Wei, R. Dickover, A. Diagne, and I. S. Chen.** 1995. Clearance of HIV infection in a perinatally infected infant. N. Engl. J. Med. **332**:833–838.
4. **Cannon, P. M., S. Matthews, N. Clark, E. D. Byles, O. Iourin, D. J. Hockley, S. M. Kingsman, and A. J. Kingsman.** 1997. Structure-function studies of the human immunodeficiency virus type 1 matrix protein, p17. J. Virol. **71**:3474–3483.
5. **Fowke, K. R., N. J. Nagelkerke, J. Kimani, J. N. Simonsen, A. O. Anzala, J. J. Bwayo, K. S. MacDonald, E. N. Ngugi, and F. A. Plummer.** 1996. Resistance to HIV-1 infection among persistently seronegative prostitutes in Nairobi, Kenya. Lancet **348**:1347–1351.
6. **Freed, E. O.** 2001. HIV-1 Replication. Somat. Cell Mol. Genet. **26**:13–33.
7. **Hamano, T., P. Sawanpanyalert, H. Yanai, S. Piyaworawong, T. Hara, S. Sapsutthipas, J. Phromjai, S. Yamazaki, N. Yamamoto, P. Warachit, M. Honda, and K. Matsuo.** 2004. Determination of HIV type 1 CRF01_AE gag p17 and env-V3 consensus sequence for HIV/AIDS vaccine design. AIDS Res. Hum. Retrovir. **20**:337–340.
8. **Huang, Y., W. A. Paxton, S. M. Wolinsky, A. U. Neumann, L. Zhang, T. He, S. Kang, D. Ceradini, Z. Jin, K. Yazdanbakhsh, K. Kunstman, D. Erickson, E. Dragon, N. R. Landau, J. Phair, D. D. Ho, and R. A. Koup.** 1996. The role of a mutant CCR5 allele in HIV-1 transmission and disease progression. Nat. Med. **2**:1240–1243.
9. **Jittiwutikarn, J., P. Sawanpanyalert, N. Pangsiveroj, and P. Satitvipawee.** 2000. HIV incidence rates among drug users in northern Thailand, 1993–7. Epidemiol. Infect. **125**:153–158.
10. **Kaul, R., T. Dong, F. A. Plummer, J. Kimani, T. Rostron, P. Kiama, E. Njagi, E. Irungu, B. Farah, J. Oyugi, R. Chakraborty, K. S. MacDonald, J. J. Bwayo, A. McMichael, and S. L. Rowland-Jones.** 2001. CD8+ lymphocytes

respond to different HIV epitopes in seronegative and infected subjects. J. Clin. Investig. **107:**1303–1310.
11. **Kober, B. T., S. Osmanov, J. Esparza, and G. Myers.** 1994. The World Health Organization Global Programme on AIDS proposal for standardization of HIV sequence nomenclature. WHO Network for HIV Isolation and Characterization. AIDS Res. Hum. Retrovir. **10:**1355–1358.
12. **Kusagawa, S., H. Sato, Y. Tomita, M. Tatsumi, K. Kato, K. Motomura, R. Yang, and Y. Takebe.** 2002. Isolation and characterization of replication-competent molecular DNA clones of HIV type 1 CRF01_AE with different coreceptor usage. AIDS Res. Hum. Retrovir. **18:**115–122.
13. **Langlade-Demoyen, P., N. Ngo-Giang-Huong, F. Ferchal, and E. Oksenhendler.** 1994. Human immunodeficiency virus (HIV) *nef*-specific cytotoxic T lymphocytes in noninfected heterosexual contact of HIV-infected patients. J. Clin. Investig. **93:**1293–1297.
14. **Learmont, J. C., A. F. Geczy, J. Mills, L. J. Ashton, C. H. Raynes-Greenow, R. J. Garsia, W. B. Dyer, L. McIntyre, R. B. Oelrichs, D. I. Rhodes, N. J. Deacon, and J. S. Sullivan.** 1999. Immunologic and virologic status after 14 to 18 years of infection with an attenuated strain of HIV-1. N. Engl. J. Med. **340:**1715–1722.
15. **Leitner, T., D. Escanilla, S. Marquina, J. Wahlberg, C. Brostrom, H. B. Hansson, M. Uhlen, and J. Albert.** 1995. Biological and molecular characterization of subtype D, G, and A/D recombinant HIV-1 transmissions in Sweden. Virology **209:**136–146.
16. **Liu, R., W. A. Paxton, S. Choe, D. Ceradini, S. R. Martin, R. Horuk, M. E. MacDonald, H. Stuhlmann, R. A. Koup, and N. R. Landau.** 1996. Homozygous defect in HIV-1 coreceptor accounts for resistance of some multiply-exposed individuals to HIV-1 infection. Cell **86:**367–377.
17. **Rein, A., L. E. Henderson, and J. G. Levin.** 1998. Nucleic-acid-chaperone activity of retroviral nucleocapsid proteins: significance for viral replication. Trends Biochem. Sci. **23:**297–301.
18. **Roldan, A., R. S. Russell, B. Marchand, M. Gotte, C. Liang, and M. A. Wainberg.** 2004. In vitro identification and characterization of an early complex linking HIV-1 genomic RNA recognition and Pr55Gag multimerization. J. Biol. Chem. **279:**39886–39894.
19. **Roques, P. A., G. Gras, F. Parnet-Mathieu, A. M. Mabondzo, C. Dollfus, R. Narwa, D. Marce, J. Tranchot-Diallo, F. Herve, G. Lasfargues, C. Courpotin, and D. Dormont.** 1995. Clearance of HIV infection in 12 perinatally infected children: clinical, virological and immunological data. AIDS **9:**F19–F26.
20. **Rowland-Jones, S. L., D. F. Nixon, M. C. Aldhous, F. Gotch, K. Ariyoshi, N. Hallam, J. S. Kroll, K. Froebel, and A. McMichael.** 1993. HIV-specific cytotoxic T-cell activity in an HIV-exposed but uninfected infant. Lancet **341:**860–861.
21. **Rowland-Jones, S., J. Sutton, K. Ariyoshi, T. Dong, F. Gotch, S. McAdam, D. Whitby, S. Sabally, A. Gallimore, T. Corrah, and M. Takiguchi.** 1995. HIV-specific cytotoxic T-cells in HIV-exposed but uninfected Gambian women. Nat. Med. **1:**59–64.
22. **Samson, M., F. Libert, B. J. Doranz, J. Rucker, C. Liesnard, C. M. Farber, S. Saragosti, C. Lapouméroulie, J. Cognaux, C. Forceille, G. Muyldermans, C. Verhofstede, G. Burtonboy, M. Georges, T. Imai, S. Rana, Y. Yi, R. J. Smyth, R. G. Collman, R. W. Doms, G. Vassart, and M. Parmentier.** 1996. Resistance to HIV-1 infection in Caucasian individuals bearing mutant alleles of the CCR-5 chemokine receptor gene. Nature **382:**722–725.
23. **Skurnick, J. H., P. Palumbo, A. DeVico, B. L. Shacklett, F. T. Valentine, M. Merges, R. Kamin-Lewis, J. Mestecky, T. Denny, G. K. Lewis, J. Lloyd, R. Praschunus, A. Baker, D. F. Nixon, S. Stranford, R. Gallo, S. H. Vermund, and D. B. Louria.** 2002. Correlates of nontransmission in US women at high risk of human immunodeficiency virus type 1 infection through sexual exposure. J. Infect. Dis. **185:**428–438.
24. **Takada, N., T. Sanda, H. Okamoto, J. P. Yang, K. Asamitsu, L. Sarol, G. Kimura, H. Uranishi, T. Tetsuka, and T. Okamoto.** 2002. RelA-associated inhibitor blocks transcription of human immunodeficiency virus type 1 by inhibiting NF-κB and Sp1 actions. J. Virol. **76:**8019–8030.
25. **Traber, K. E., H. Okamoto, C. Kurono, M. Baba, C. Saliou, T. Soji, L. Packer, and T. Okamoto.** 1999. Anti-rheumatic compound aurothioglucose inhibits tumor necrosis factor alpha-induced HIV-1 replication in latently infected OM10.1 and Ach2 cells. Int. Immunol. **11:**143–150.
26. **Zhu, T., L. Corey, Y. Hwangbo, J. M. Lee, G. H. Learn, J. I. Mullins, and M. J. McElrath.** 2003. Persistence of extraordinarily low levels of genetically homogeneous human immunodeficiency virus type 1 in exposed seronegative individuals. J. Virol. **77:**6108–6116.

PNAS
Proceedings of the National Academy of Sciences of the United States of America www.pnas.org

Aberrant MHC class II expression in mouse joints leads to arthritis with extraarticular manifestations similar to rheumatoid arthritis

Satoshi Kanazawa, Shusuke Ota, Chiyoko Sekine, Toyohiro Tada, Takanobu Otsuka, Takashi Okamoto, Grete Sønderstrup, and B. Matija Peterlin

PNAS 2006;103;14465-14470; originally published online Sep 15, 2006;
doi:10.1073/pnas.0606450103

Aberrant MHC class II expression in mouse joints leads to arthritis with extraarticular manifestations similar to rheumatoid arthritis

Satoshi Kanazawa[†], Shusuke Ota[†], Chiyoko Sekine[‡], Toyohiro Tada[§], Takanobu Otsuka[¶], Takashi Okamoto[†‖], Grete Sønderstrup[††], and B. Matija Peterlin[‖‡‡]

Departments of [†]Molecular and Cellular Biology and [¶]Musculoskeletal Medicine, Nagoya City University Graduate School of Medical Sciences, 1 Kawasumi, Mizuho-cho, Nagoya 467-8601, Japan; [‡]Research Unit for Clinical Immunology, Riken Research Center for Allergy and Immunology, Tokyo 230-0045, Japan; [§]Department of Pathology, Nagoya City University Graduate School of Nursing, Nagoya 467-8601, Japan; [††]Departments of Microbiology and Immunology, Stanford University School of Medicine, Stanford, CA 94305-5124; and [‡‡]Rosalind Russell Medical Research Center, Departments of Medicine, Microbiology, and Immunology, University of California, San Francisco, CA 94143-0703

Communicated by Hugh O. McDevitt, Stanford University School of Medicine, Stanford, CA, August 1, 2006 (received for review April 17, 2006)

Genetic susceptibility to rheumatoid arthritis (RA) is associated with certain MHC class II molecules. To clarify the role of these determinants in RA, we generated the D1CC transgenic mouse that expressed genes involved in antigen processing and presentation by the MHC class II pathway in joints. The class II transactivator, which was transcribed from the rat collagen type II promoter and enhancer, directed the expression of these genes. In D1CC mice congenic for the H-2^q (DBA/1) background, small amounts of bovine collagen type II in adjuvant induced reproducibly an inflammatory arthritis resembling RA. Importantly, these stimuli had no effect in DBA/1 mice. Eighty-nine percent of D1CC mice developed chronic disease with joint swelling, redness, and heat in association with synovial proliferation as well as pannus formation and mononuclear infiltration of synovial membranes. Granulomatous lesions resembling rheumatoid nodules and interstitial pneumonitis also were observed. As in patients with RA, anticyclic citrullinated peptide antibodies were detected during the inflammatory stage. Finally, joints in D1CC mice displayed juxtaarticular demineralization, severe joint space narrowing, and erosions, which led to ankylosis, but without the appearance of osteophytes. Thus, aberrant expression of MHC class II in joints facilitates the development of severe erosive inflammatory polyarthritis, which is very similar to RA.

autoimmunity | class II transactivator | transgenic mouse | nodules | pneumonitis

Rheumatoid arthritis (RA) is a chronic inflammatory disease with symmetrical inflammatory and erosive polyarthritis of synovial joints and a variety of extraarticular manifestations. Particular MHC class II alleles such as DRB0401, DRB0404, and DQ8 are linked to RA in 30–50% of cases (1–3). To examine possible mechanisms of RA, many models of inflammatory arthritis have been developed in the mouse and rat (4, 5). Among these models, collagen-induced arthritis (CIA) leads to acute inflammation, osteophytosis, and destruction of bone in DBA/1 and B10.Q (H2^q) strains of mice (6, 7). In these mice, passively transferred autoantibodies against CII, or the injection of a combination of certain monoclonal anti-CII antibodies, also induce rapid inflammation of joints (8, 9). A recently discovered model, the SKG mouse, contains mutations in the ζ chain-associated protein of 70 kDa (ZAP-70) that is involved in the signaling from the T cell antigen receptor (10). In these mice, infection with fungi or immunization with zymosan can induce a chronic inflammatory arthritis (11). In K/BxN mice, chronic arthritis develops spontaneously because anti-G6PI antibodies accumulate in serum and joints, leading to inflammatory arthritis and bone destruction (12, 13). In all these mice and several other models, the onset and progression of inflammatory arthritis have been well characterized and analyzed. However, how faithfully these small animal models resemble RA and what roles MHC class II play in their disease have remained elusive.

MHC class II, DM, and invariant chain (Ii) genes are all regulated at the transcriptional level by the class II transactivator (CIITA) (14). These genes share cis-acting sequences (S, X, and Y boxes) in their promoters and enhancers that bind regulatory factor X (RFX) and nuclear factor (NF-Y) that, in turn recruit CIITA (15, 16). CIITA then binds many coactivators that increase rates of initiation and elongation of MHC class II, DM, and Ii genes. RFX and NF-Y are expressed ubiquitously. In sharp contrast, the expression of CIITA is restricted to antigen-presenting cells and mature B cells (17). Thus, CIITA is the master transcriptional integrator that leads to the expression of genes required for antigen processing and presentation by the MHC class II pathway. Interestingly, the cytokine IFN-γ induces the synthesis of CIITA and, thereby, of MHC class II in many somatic cells, which transforms them to "professional" antigen-presenting cells at sites of inflammation (18).

To determine whether the aberrant expression of MHC class II in joints can lead to or potentiate inflammatory arthritis in mice, we linked the human CIITA gene to the rat CII promoter and enhancer (19). This plasmid construction then was used to create transgenic DBA/1, CII promoter/enhancer-driven CIITA (D1CC) mice, which were analyzed further.

Results

D1CC Mice Express MHC Class II in Joints and Are Highly Susceptible to Immunization with Low Doses of Bovine CII (bCII). D1CC mice express CIITA and MHC class II in joints (Fig. 6, which is published as supporting information on the PNAS web site). Although spontaneous swelling and redness would occur in isolated joints of most mice, D1CC mice did not develop chronic symmetrical polyarthritis. Similar to SKG and DBA/1 mice (CIA model), the D1CC mice required a trigger to develop inflammatory arthritis. However, because of the aberrant expression of MHC class II in joints, we expected the D1CC mice to be more responsive to the immunization with bCII than parental DBA/1 mice. Thus, we tested progressively lower doses

Author contributions: S.K., T. Okamoto, G.S., and B.M.P. designed research; S.K., S.O., C.S., T.T., and T. Otsuka performed research; S.K., T. Okamoto, G.S., and B.M.P. contributed new reagents/analytic tools; S.K., T. Okamoto, G.S., and B.M.P. analyzed data; and S.K., T. Okamoto, G.S., and B.M.P. wrote the paper.

The authors declare no conflict of interest.

Abbreviations: CII, collagen type II; bCII, bovine CII; hiCII, high-dose bCII; loCII, lower doses of bCII; CIITA, class II transactivator; CCP, cyclic citrullinated peptide; CIA, collagen-induced arthritis; CT, computed tomographic; D1CC, DBA/1, CII promoter/enhancer-driven CIITA; RA, rheumatoid arthritis.

‖To whom correspondence may be addressed. E-mail: tokamoto@med.nagoya-cu.ac.jp or matija.peterlin@ucsf.edu.

of bovine CII (loCII) in D1CC mice. We used the clinical score in Table 1, which is published as supporting information on the PNAS web site, to monitor the development of inflammatory arthritis (6). Indeed, the D1CC mice developed severe CIA after immunization with 5–10 μg of bCII (loCII-D1CC), a dose that never elicited detectable disease in DBA/1 mice (loCII-DBA/1; Fig. 1*A*). Thus, the conventional DBA/1 control mice required 20- to 40-fold higher amounts of bCII [200 μg of bCII, high-dose bCII (hiCII)] for the induction of CIA (hiCII-DBA/1, Fig. 1*A*).

The incidence of disease between sexes was not statistically different (data not presented). Moreover, in loCII-D1CC mice, the peak clinical score of inflammatory arthritis was the same as in hiCII-DBA/1 mice. However, the inflammatory period lasted 34.3 ± 3.7 days in loCII-D1CC mice versus 15.9 ± 2.7 days in hiCII-DBA/1 mice (Fig. 1*A*). Thus, the duration of inflammation was twice as long in loCII-D1CC mice. The Mann–Whitney *U* test was used to confirm the significance of this difference ($P < 0.01$). In addition, the disease incidence was increased from 57.1% in hiCII-DBA/1 mice to 89% in loCII-D1CC or hiCII-D1CC mice (Table 2, which is published as supporting information on the PNAS web site). Whereas redness and swelling were severe in loCII-D1CC mice, no obvious clinical symptoms were observed in loCII-DBA/1 mice (Fig. 1 *B–E*). We also examined temperatures at various limbs by thermography. Temperatures averaged ≈25°C in loCII-DBA/1 mice and increased up to 28°C in loCII-D1CC mice (Fig. 1 *F* and *G* and thermographs below). Taken together, D1CC mice developed chronic inflammatory arthritis with redness, swelling, and fever at the joint after immunization with minimal amounts of bCII. This finding indicates that the aberrant expression of MHC class II in synovial joints facilitates the development of chronic inflammatory arthritis in the D1CC mouse.

Histological Features of Articular Inflammation in loCII-D1CC Mice. We also examined the progression of disease by histology. At 1 week after the second immunization, there was no inflammation in loCII-DBA/1 mice (Fig. 2 *A* and *D* and data not shown). At 8 weeks, infiltration of inflammatory cells, proliferation of synoviocytes with pannus formation, and erosion of bone were observed exclusively in loCII-D1CC, but not loCII-DBA/1 mice (Fig. 2 *B* and *E*). In the loCII-D1CC mice, the number of infiltrating cells declined dramatically at 15 weeks (Fig. 2*C*). However, an abundance of granulocytes (Fig. 2*C*) and mast cells (Fig. 7, which is published as supporting information on the PNAS web site) had migrated into the pannus at that point, and although the subchondral articular cartilage was severely disrupted at this stage, no subluxation and/or ankylosis was detected until much later. We also found granulomatous lesions resembling rheumatoid nodules in loCII-D1CC but not in loCII-DBA/1 mice (Fig. 2 *G* and *H*).

Interstitial Pneumonitis in loCII-D1CC Mice. We found interstitial pneumonitis with fibrosis as an extraarticular manifestation of disease only in loCII-D1CC but not in hiCII-DBA/1 mice >6 months after the first immunization (Fig. 3 *B* and *D*). There was also a sizeable infiltration of mononuclear cells such as neutrophils and macrophages in these pulmonary lesions. However, because the mice were kept under specific pathogen-free (SPF) conditions and we did not find the deposition of fibrin in D1CC or DBA/1 mice, there was no indication that this inflammation could be due to infection (Fig. 3 *A* and *C*). However, newly synthesized elastic fibers were identified in loCII-D1CC mice by elastica and Kernechtrot staining (Fig. 3*B*). Because interstitial pneumonitis has not been described with CIA but can be found in severe RA, this feature again documents the similarities in inflammatory lesions between loCII-D1CC mice and RA in humans.

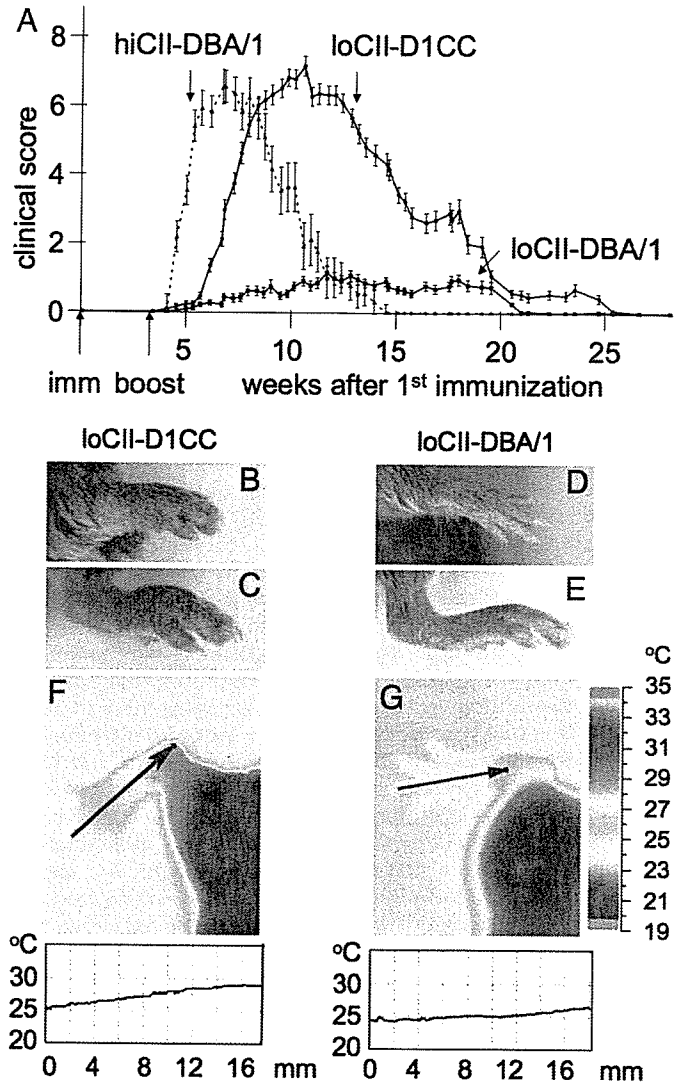

Fig. 1. Chronic arthritis in the loCII-D1CC mouse. To compare D1CC and DBA/1 mice receiving loCII or hiCII, clinical pictures of each mouse were monitored twice weekly and scored (Table 1). Eight-week-old mice were injected with bCII/complete Freund's adjuvant and boosted with bCII/incomplete Freund's adjuvant 3 weeks later (arrows below the graph). (*A*) loCII-D1CC but not loCII-DBA/1 mice develop polyarthritis, which persists for a longer period. Graphs are as follows: Line with filled circles, D1CC mouse injected with loCII (loCII-D1CC); bold line with filled squares, DBA/1 mice injected with loCII (loCII-DBA/1); dashed line with filled triangles: DBA/1 mice injected with hiCII (hiCII-DBA/1). Eighty-nine percent of loCII-D1CC but only 57% of hiCII-DBA.1 mice developed arthritis. Our clinical criteria focused on heat, swelling, redness, and functional impairment. (*B–E*) Joints of loCII-D1CC mouse are swollen. Although parental DBA/1 mice had no phenotype on loCII (*D* and *E*, fore limbs and hind limbs, respectively), loCII-D1CC mice developed swollen and red extremities on this regiment (*B* and *C*, fore limbs and hind limbs, respectively). (*F* and *G*) Joints of loCII-D1CC mouse are hot. Thermographs were performed with joints of loCII-D1CC and loCII-DBA/1 mice. Whereas the maximum temperature at the foot reached 25°C in average in the loCII-DBA/1 mouse (*G*), it reached 28°C on average in the loCII-D1CC mouse at 8 weeks (*F*). Arrows in *F* and *G* point in the direction of thermographs, from arrow point to arrowhead. Numbers below the graph indicate the distance from arrow point in millimeters. The thermal scale with corresponding temperatures (°C) is presented as colors changing from blue to red to the right of *G*.

Bone Destruction and Decreased Mineral Density in loCII-D1CC Mice. Next, we demonstrated the severity of articular pathology by radiography. In loCII-D1CC mice, decreased mineral density was observed at 18 and 39 weeks after the immunization but not at earlier stages of inflammation (Fig. 4 *A–D*). To substantiate

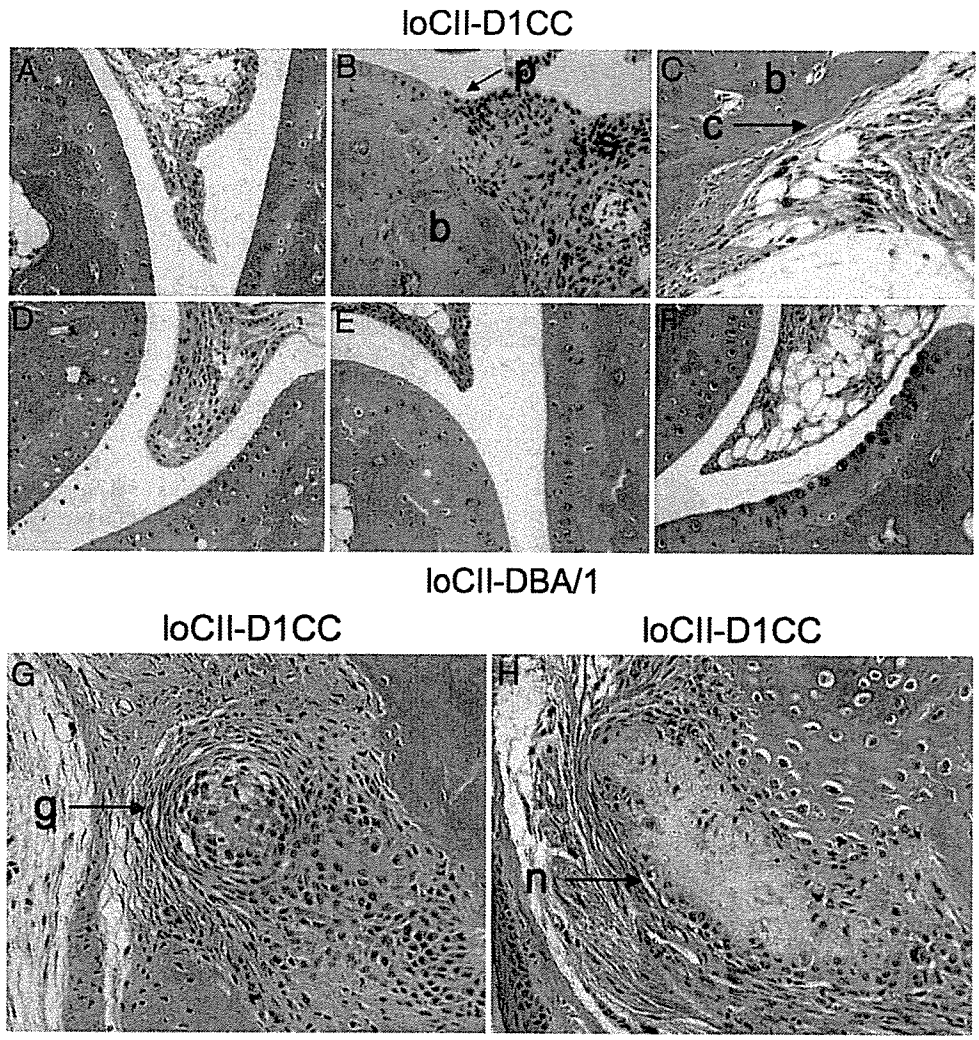

Fig. 2. Histology of the loCII-D1CC mouse. (*A–C*) Histology of joints from the loCII-D1CC mouse. Although no changes are observed 1 week after the boost (*A*), pannus formation over articular cartilage and proliferating synoviocytes (p and s, respectively; *B*), and thinning of articular cartilage (c; *C*) are observed at 8 and 15 weeks after the boost, respectively. Bone (b) also is labeled. (*D–F*) Histology of joints in the loCII-DBA/1 mouse shows no changes at 1 (*D*), 8 (*E*), and 15 (*F*) weeks after the boost. (*G* and *H*) Nodules are observed in the loCII-D1CC mouse. Three weeks after the boost, granulomas (g; *G*) and nodules (h; *H*) are observed only in the loCII-D1CC mouse.

further these radiographic findings, we also performed computed tomographic (CT) scans focused on the large knee joints. Bone destruction, joint space narrowing, and erosions were observed at the patella, distal femur, proximal tibia, and fibula (Fig. 4 *E–J*; see Movies 1–3, which are published as supporting information on the PNAS web site). In addition, relatively dark-gray areas that represent decreased mineral densities paralleled the progression of bone erosions. Osteophytes and "rebound" new bone formation such as arthrodysplasia were found only in hiCII-DBA/1 mice (Fig. 4 *I* and *J* and Movies 1–3) (7). To confirm the osteoporosis at the knee joint, the bone mineral density of cancellous bone in each mouse was calculated from CT scan data. The bone mineral density declined immediately after immunization in hiCII-DBA/1 mice (Fig. 4*K*). It decreased by ≈10% and then recovered at 3 months. In contrast, it decreased by 25% at 3 months and lasted at least 6 months in loCII-D1CC mice. At the terminal stage of chronic inflammatory arthritis, severe ankylosis also was observed at the proximal interphalangeal and metacarpophalangeal joints in loCII-D1CC mice (Fig. 5 *A* and *B*). Even though they were observed for >1 year, we did not detect any osteoporosis or bone erosions in loCII-DBA/1 mice. Thus, the articular deterioration of the loCII-D1CC mouse, in contrast to that of CIA, seems to be chronic and progressive, similar to the joint destruction seen in severe active RA.

Discussion

In this report, we present the D1CC small animal model of inflammatory arthritis. In these mice, the entire machinery for antigen processing and presentation by the MHC class II pathway was activated aberrantly via transgenic expression of CIITA. First, the D1CC mice containing ≈10 copies of the CIITA transgene expressed easily detectable CIITA transcripts and MHC class II in joints (Fig. 6). Second, chronic inflammatory arthritis developed in 89% of male and female loCII-D1CC mice (as contrasted to 57% of CIA in hiCII-DBA/1 mice) after immunization with small doses of bCII that had no effect on parental DBA/1 mice. Third, not only did this arthritis start slower and last longer than CIA in hiCII-DBA/1 mice, but it resulted in characteristic articular and extraarticular manifestations very closely resembling those of severe RA in humans. In loCII-D1CC mice, chronic symmetrical polyarthritis eventually led to ankylosis and destruction of affected joints. Finally, as in RA, D1CC mice developed antibodies to CCP (Table 3, which

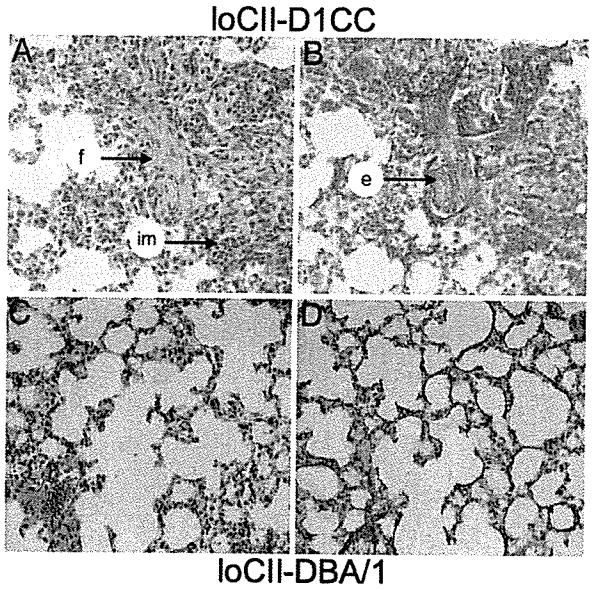

Fig. 3. Interstitial pneumonitis is observed only in loCII-D1CC mice. Histology of lungs 6 months after the boost in loCII-D1CC and loCII-DBA/1 mice. Fibrosis, infiltrating mononuclear cells (f and im, arrow, respectively; *A*), and newly produced elastic fiber (e, arrow; *B*) are observed in lungs of the loCII-D1CC mouse but not in those of the loCII-DBA/1 mouse (*C* and *D*). *A* and *C* were stained with HE. *B* and *D* were stained with elastica and kernechtrot stains to visualize elastic fibers.

is published as supporting information on the PNAS web site). Importantly, unlike other models of inflammatory arthritis (5), we did not introduce any mutations into the mouse. Thus, our work returns the emphasis of RA back to the normal and aberrant immune responses in the host. We propose that D1CC mice may represent an attractive additional animal model for the study of RA.

Histologically, inflammatory infiltrates and proliferating synoviocytes leading to granulomatous lesions resembling rheumatoid nodules were observed only in loCII-D1CC mice. Even though the presence of palisading histiocytes surrounding necrotic nodules could not be ascertained, similar pathology has been reported with pristane-induced arthritis, MRL-lpr/lpr, and SKG mice but not with CIA in DBA/1 mice (11, 20, 21). In contrast to the SKG mice, the D1CC mice had no skin inflammation. Slowly progressive inflammatory arthritis also led to easily identifiable migration of mast cells into the pannus. Because these mast cells expressed MHC class II and B7.1, they might potentially function as antigen-presenting cells (Fig. 7; refs. 22 and 23).

We also observed interstitial pneumonitis with fibrosis and deposition of newly synthesized elastic fibers in the lungs of loCII-D1CC mice. These lesions lacked fibrin, which can be related to infection. Serological analyses revealed the presence of anti-CII and CCP antibodies in sera of both loCII-D1CC and hiCII-DBA/1 mice (Table 3). Notably, the concentration of anti-CCP antibodies was significantly higher in loCII-D1CC than in hiCII-DBA/1 mice, suggesting a more sustained inflammatory process in joints of loCII-D1CC mice. However, attempts to measure the concentration of cytokines and anti-CII antibodies in the synovial fluid were not successful. Radiographic examinations and CT scans revealed further similarities between the arthritis in the loCII-D1CC mouse and RA. These data included periarticular osteoporosis, joint space narrowing, and severe destruction of bone without osteophytosis, all of which led eventually to ankylosis. Although the erosive destruction of bone started in the earlier stages of inflammation at 8 weeks, this bone erosion could only be detected by histology and not yet radiographically (Figs. 2*B* and 4 *A–D* and *K*). Recently, similar microscopic joint damage was detected by MRI in RA patients (24–26).

In a subgroup of RA patients, MHC class II represent a critical genetic risk factor for the susceptibility to the disease (27). Moreover, the expression of these HLAs (HLA class II) have been detected in chondrocytes of RA patients (28, 29). From our study, we hypothesize that the expression of MHC class II on target organs can increase their sensitivity to arthritogenic stimuli in general. This observation might explain the spontaneous inflammation of individual joints without immunization in D1CC mice, some of which persisted for prolonged periods of time and could have resulted from local trauma (data not presented). Moreover, increased sensitivity also might explain the rather severe bone destruction we found in loCII-D1CC mice. In contrast, acute inflammation induces osteophytosis in CIA in DBA/1 mice, where bone resorption is more transient and new bone formation is enhanced soon thereafter (7, 30). Finally, joints in loCII-D1CC but not loCII-DBA/1 progressed to ankylosis and severe functional impairment. We found severe bone destruction in almost all metacarpophalangeal joint and in >60–80% of the proximal interphalangeal joints. These data suggest that lower doses of bCII lead to a more chronic arthritis in the more susceptible D1CC than DBA/1 mice, which is reminiscent of a slow smoldering course of progressive joint destruction seen in severe RA (4, 31).

D1CC mice also provide an excellent breeding partner for other models of inflammatory arthritis in the mouse. Because the balance between Th1 and Th2 was not significantly different in D1CC mice, aberrant expression of MHC class II together with abnormal selection of T cells such as survival of autoreactive clones will be investigated further. For example, the hCIITA transgene also might influence other types of arthritis in mice and possibly render the arthritis in other animal models, such as SKG mouse, spontaneous (20, 32, 33). Moreover to create even better and more mouse models of RA, D1CC mice may be backcrossed with the DRB1*0401 or DRB1*0402, and human CD4 double-transgenic mice, which lack I-A$\beta^{-/-}$ on the DBA/1 background (34, 35). Both DR genes are expressed from the mouse I-Eα promoter and enhancer, thus aberrant CIITA expression will induce the expression of DR*0401 or DRB1*0402 in their chondrocytes (36). DRB1*0401 is not only one of the susceptible genes for RA but is also the molecule that presents citrullinated arthritogenic antigens. However, DRB1*0402 does not present the same peptides. Thus, these DR alleles will help us to dissect the contributions between specific arthritogenic stimuli and MHC class II from RA patients. Also, specific peptides that are presented by aberrantly expressed MHC class II in humanized D1CC mice will be used to tolerize these mice to these antigens, which then can be evaluated for effects of such therapeutic vaccination on their disease.

Materials and Methods

CIA. For the induction of CIA, D1CC and DBA/1 mice at 7 to 9 weeks of age were housed in a pathogen-free animal care facility of Nagoya City University Graduate School of Medical Sciences in accordance with institutional guidelines. These mice were anesthetized with diethyl ether before induction of CIA. At that point, they were immunized with bCII (5–10 μg, called loCII for D1CC and DBA/1 mice and 200 μg, called hiCII for DBA/1 mice) (Collagen Research Center, Tokyo, Japan), which was emulsified with an equal volume of complete Freund's adjuvant (Difco Laboratories, Detroit, MI). Mice were injected intradermally at the base of the tail, near inguinal and axillary lymph nodes on day 0 as the first injection. On day 21, the mice were boosted with the bCII in the same manner except that incom-

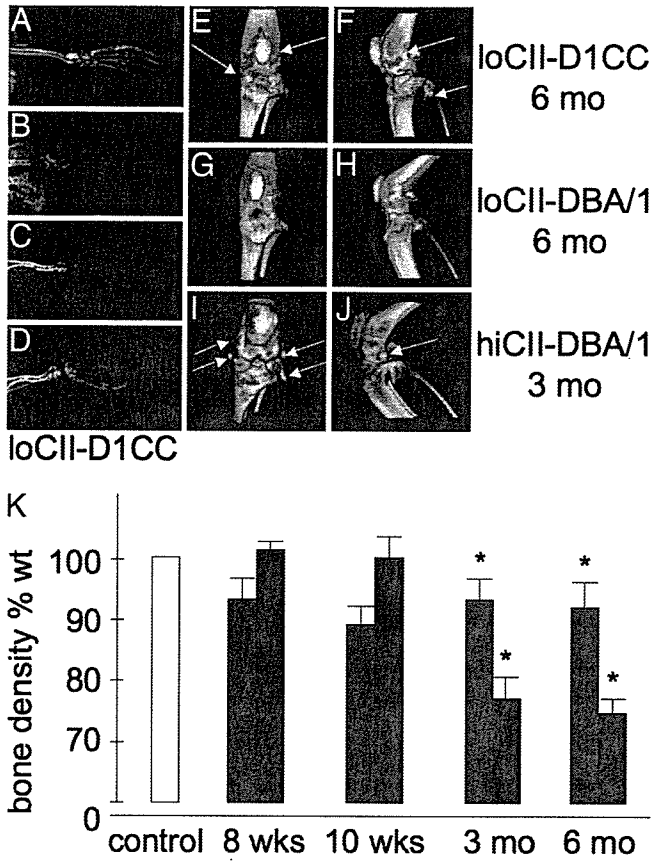

Fig. 4. Joint space narrowing, erosions, and osteoporosis in the loCII-D1CC mouse. (*A–D*) Progressive joint damage in the loCII-D1CC mouse. Radiographic examination reveals the decline of bone mineral density and joint space narrowing and erosions in the fore limbs at 0 (*A*), 9 (*B*), 18 (*C*), and 39 (*D*) weeks after the first injection. (*E–J*) Joint space narrowing, erosions, and osteoporosis in the knee of the loCII-D1CC mouse 24 weeks after the boost. (*E* and *F*) CT scans are presented for the distal femur, the knee joint, the proximal tibia, and the fibula. Note the narrowing of the joint space (*E*, left arrow), erosions, and osteoporosis (*E* and *F*, right arrows). None of these changes are observed in the parental loCII-DBA/1 mouse treated likewise (*G* and *H*). In sharp contrast, hiCII-DBA/1 mice developed erosions and formed new bone resembling osteophytes 12 weeks after the boost (*I* and *J*, arrows). (*K*) Progressive osteoporosis in the loCII-D1CC mouse. Presented is the comparison of decreased periarticular bone mineral density over time between ldCII-D1CC and hiCII-DBA/1 mice. Ten sections of cancellous bone measuring 0.1 mm each were analyzed by densitometry of CT scans from both knees in each mouse. Times after the boost are presented below the bar graphs. Data are presented as percentage of bone mineral density of loCII-D1CC (black bars) and hiCII-DBA/1 (gray bars) compared with the untreated parental DBA/1 mouse (WT was given the value of 100%; open bar) over time. Six mice were studied in each group. Error bars reflect SEM. All values were calculated by using data from three or four mice. Student's *t* test was performed for each value between loCII-D1CC and hiCII-DBA/1 mice (*, $P < 0.05$).

plete Freund's adjuvant (Difco Laboratories) was used as the solvent.

Evaluation of Joint Arthritis. DBA/1 and D1CC mice were monitored from the onset of disease to the end of active inflammation twice weekly. The clinical severity of arthritis was quantified according to this simple scoring system: 0, no clinical symptom; 1, swelling and redness of one or two joints; 2, moderate swelling and redness of more than three joints; 3, severe swelling and redness of entire paw (6). All scores were added to the total clinical score, which reached the maximum at 12 (four severely affected joints, 4 × 3). The onset of arthritis was defined as the

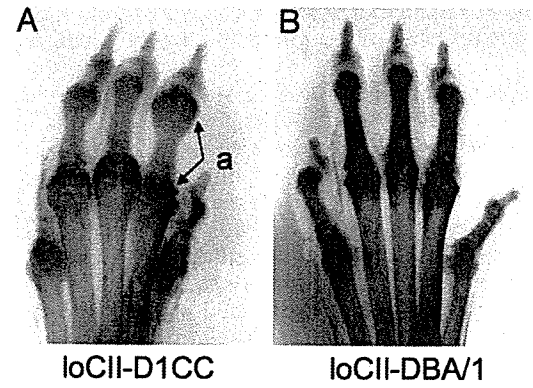

Fig. 5. Fore limbs of the loCII-D1CC mouse reveal extensive joint destruction. Fifteen months after the boost, fore limbs of loCII-D1CC (*A*) and loCII-DBA/1 (*B*) mice were stained with Alizarin and Alcian blue, which stain bone red and cartilage blue. Note the complete destruction of all joints (ankylosis, a, arrows) and shortening of phalanges in the loCII-D1CC mouse and normal joints in loCII-DBA/1 mice.

number of days between the first immunization with bCII and the occurrence of arthritis with a clinical score of >3. The end of acute arthritis was noted when the clinical score was reduced to 3. Body temperatures were measured at all extremities by using the thermograph (Neo Thermo; Nippon Anionics, Tokyo, Japan).

Immunohistochemistry. For immunohistochemical staining, the avidin–biotin–peroxidase complex (ABC) method was used according to protocols from the manufacturer (Vector Laboratories, Burlingame, CA) (37). Paraffin sections were rehydrated and washed with tap water for 5 min. The endogenous peroxidase activity was inhibited by first incubating samples in 0.05% of H_2O_2 solution for 30 min and then washing with PBS for 10 min at room temperature. Thin sections were incubated with buffer C (1.5% normal serum in PBS) for 60 min, and primary antibodies (biotin-conjugated mouse anti-mouse I-A^q monoclonal antibody, BD Biosciences, San Jose, CA) were diluted to 1:6 with the blocking buffer (supplied by Vector Laboratories) for 30 min and washed with PBS for 10 min. All incubation steps with antibodies were performed in a humid chamber. Signals were detected by using a commercial ABC kit and DAB solution (Mouse on Mouse Immunodetection kits PK-2200 and SK-4100, respectively; Vector Laboratories). All specimens were counterstained with hematoxylin and mounted in VectaMount (H-5000; Vector Laboratories). As the negative control, isotype-matched antibodies (biotin-conjugated mouse IgG_{2b}, monoclonal Ig isotype control; BD Biosciences Pharmingen) were used.

Radiographic Technique. The computed radiographs (CR) were obtained by using the CR console (FCR5000plus; Fujifilm, Tokyo, Japan) and the high-resolution CR cassette (Fujifilm). The source of x-rays was a conventional radiographic unit and exposure factors were 50 kV, 50 mA, and 40 ms (Shimadzu, Kyoto, Japan).

Bone Mineral Density and CT. We used peripheral quantitative computed tomography with a fixed x-ray fan beam of 10-mm spot size, at 1 mA and 50kVp (LaTheta LCT-100S; Aloka, Tokyo, Japan). Eighty slices (480 × 480-pixel matrix per slice, 0.1 mm thickness, a voxel size of 65 × 65 × 65 μm^3) covered the entire knee joint and recreated the 3D CT picture of the joint by using the VGStudio MAX1.2 software (Nihon Visual Science, Tokyo, Japan). To measure the mineral density of bones at the joint

from each mouse, data were recalculated from the distal femur and the proximal tibia, both adjoining the articular cartilage.

Histochemical Staining. For H&E staining, paraffin sections were rehydrated and immersed first into the Mayer's hematoxylin solution (Muto Pure Chemicals Co., Ltd., Tokyo, Japan) for 5 min and then into the eosin solution (Muto Pure Chemicals Co., Ltd.) for 2 min. For elastical and kernechtrot staining, paraffin sections also were rehydrated. After washing with 1% of hydrochloric acid and 70% ethanol for 5 min, sections were incubated with resorcin fuchsin solution (Muto Pure Chemicals Co., Ltd.) for 60 min, washed with ethanol, and counterstained with Kernechtrot stain solution (Muto Pure Chemicals Co., Ltd.) for 2 min. For toluidine blue staining, sections were rehydrated and washed with tap water for 5 min and incubated with 0.05% of toluidine blue O solution (Waldeck, Muenster, Germany) for 10 min. All sections were dehydrated with ethanol and mounted in VectaMount. To count the number of infiltrated mast cells in the joint, the five most-visible areas of mast cells were selected in toluidine blue stained histological slides. The number of mast cells then were counted in all extremities in D1CC and DBA/1 mice and visualized in a bar graph. For cartilage and bone staining, specimens were immersed in 95% of ethanol for >5 days and in acetone for another 2 days. Skin, muscle, and fat were removed carefully and stained with Alcian blue (0.3% of Alcian blue 8GX; Sigma–Aldrich, St. Louis, MO) and Alizarin red (0.1% Alizarin sodium monosulfonate; Sigma–Aldrich) for 3 days. Finally, specimens were immersed in the 1% KOH solution and glycerol for 2 days.

Statistical Analyses. All measurements were performed in duplicate, and all experiments were repeated at least three times. All error bars give SEM. Mann–Whitney U test was used for the statistical analysis of disease-related parameters between control and arthritic mice. The histomorphometric data and the serum titers of anti-CII antibodies between the control and the arthritic mice were compared by Student's t test. Values of $P < 0.05$ were considered to be statistically significant.

Supporting Information. Additional data can be found in *Supporting Materials and Methods*, which is published as supporting information on the PNAS web site.

We thank M. Vadeboncoeur for the generation of D1CC mice; S. Fujii, K. Yuzawa, M. Sakamoto, Y. Miyahara, and S. Imai for outstanding technical support; H. Otsuka and Y. Tachikawa for quantitative CT analyses (Aloka, Tokyo, Japan); and William Seaman and Hugh O. McDevitt for critical discussions and comments on the manuscript. This work was supported by grants-in-aid from the Ministry of Health, Labor, and Welfare and Ministry of Education, Culture, Sports, Science, and Technology (Japan), and the Nora Eccles Treadwell Foundation and National Institutes of Health Grants R01 AI050770 and AR44647.

1. van Zeben D, Hazes JM, Zwinderman AH, Cats A, Schreuder GM, D'Amaro J, Breedveld FC (1991) *Arthritis Rheum* 34:822–830.
2. Feldmann M, Brennan FM, Maini RN (1996) *Cell* 85:307–310.
3. Silman AJ, Pearson JE (2002) *Arthritis Res* 4(Suppl 3):S265–S272.
4. Firestein GS (2004) *J Clin Invest* 114:471–474.
5. Monach PA, Benoist C, Mathis D (2004) *Adv Immunol* 82:217–248.
6. Wooley PH, Luthra HS, Stuart JM, David CS (1981) *J Exp Med* 154:688–700.
7. Hanyu T, Chotanaphuti T, Arai K, Tanaka T, Takahashi HE (1999) *Bone* 24:485–490.
8. Holmdahl R, Jansson L, Larsson A, Jonsson R (1990) *Scand J Immunol* 31:147–157.
9. Terato K, Hasty KA, Reife RA, Cremer MA, Kang AH, Stuart JM (1992) *J Immunol* 148:2103–2108.
10. Sakaguchi N, Takahashi T, Hata H, Nomura T, Tagami T, Yamazaki S, Sakihama T, Matsutani T, Negishi I, Nakatsuru S, Sakaguchi S (2003) *Nature* 426:454–460.
11. Yoshitomi H, Sakaguchi N, Kobayashi K, Brown GD, Tagami T, Sakihama T, Hirota K, Tanaka S, Nomura T, Miki I, *et al.* (2005) *J Exp Med* 201:949–960.
12. Korganow AS, Ji H, Mangialaio S, Duchatelle V, Pelanda R, Martin T, Degott C, Kikutani H, Rajewsky K, Pasquali JL, *et al.* (1999) *Immunity* 10:451–461.
13. Matsumoto I, Staub A, Benoist C, Mathis D (1999) *Science* 286:1732–1735.
14. Fontes JD, Kanazawa S, Nekrep N, Peterlin BM (1999) *Microbes Infect* 1:863–869.
15. Jabrane-Ferrat N, Fontes JD, Boss JM, Peterlin BM (1996) *Mol Cell Biol* 16:4683–4690.
16. Zhu XS, Linhoff MW, Li G, Chin KC, Maity SN, Ting JP (2000) *Mol Cell Biol* 20:6051–6061.
17. Kanazawa S, Peterlin BM (2001) *Microbes Infect* 3:467–473.
18. Steimle V, Siegrist CA, Mottet A, Lisowska-Grospierre B, Mach B (1994) *Science* 265:106–109.
19. Horton W, Miyashita T, Kohno K, Hassell JR, Yamada Y (1987) *Proc Natl Acad Sci USA* 84:8864–8868.
20. Wooley PH, Seibold JR, Whalen JD, Chapdelaine JM (1989) *Arthritis Rheum* 32:1022–1030.
21. Hang L, Theofilopoulos AN, Dixon FJ (1982) *J Exp Med* 155:1690–1701.
22. Lee DM, Friend DS, Gurish MF, Benoist C, Mathis D, Brenner MB (2002) *Science* 297:1689–1692.
23. Tetlow LC, Woolley DE (1995) *Ann Rheum Dis* 54:896–903.
24. Forslind K, Larsson EM, Eberhardt K, Johansson A, Svensson B (2004) *Scand J Rheumatol* 33:154–161.
25. Ostergaard M, Ejbjerg B, Szkudlarek M (2005) *Best Pract Res Clin Rheumatol* 19:91–116.
26. Guermazi A, Taouli B, Lynch JA, Peterfy CG (2004) *Semin Musculoskelet Radiol* 8:269–285.
27. Ridgway WM, Fasso M, Fathman CG (1999) *Science* 284:749:751.
28. Allard SA, Muirden KD, Camplejohn KL, Maini RN (1987) *Rheumatol Int* 7:153–159.
29. Lance EM, Kimura LH, Manibog CN (1993) *Clin Orthop Relat Res* 291:266–282.
30. Enokida M, Yamasaki D, Okano T, Hagino H, Morio Y, Teshima R (2001) *Bone* 28:87–93.
31. Weyand CM, Hicok KC, Conn DL, Goronzy JJ (1992) *Ann Intern Med* 117:801–806.
32. Keystone EC, Schorlemmer HU, Pope C, Allison AC (1977) *Arthritis Rheum* 20:1396–1401.
33. Eming R, Visconti K, Hall F, Sekine C, Kobayashi K, Chen Q, Cope A, Kanazawa S, Peterlin M, Rijnders A, *et al.* (2002) *Arthritis Res* 4(Suppl 3):S133–S140.
34. Sonderstrup G (2003) *Springer Semin Immunopathol* 25:35–45.
35. Fugger L, Michie SA, Rulifson I, Lock CB, McDevitt GS (1994) *Proc Natl Acad Sci USA* 91:6151–6155.
36. Kouskoff V, Fehling HJ, Lemeur M, Benoist C, Mathis D (1993) *J Immunol Methods* 166:287–291.
37. Ando K, Kanazawa S, Tetsuka T, Ohta S, Jiang X, Tada T, Kobayashi M, Matsui N, Okamoto T (2003) *Oncogene* 22:7796–7803.

THE JOURNAL OF BIOLOGICAL CHEMISTRY VOL. 281, NO. 18, pp. 12495–12505, May 5, 2006

Transcriptional Repression of Human Immunodeficiency Virus Type 1 by AP-4*

Received for publication, November 1, 2005, and in revised form, March 14, 2006 Published, JBC Papers in Press, March 15, 2006, DOI 10.1074/jbc.M511773200

Kenichi Imai and Takashi Okamoto[1]

From the Department of Molecular and Cellular Biology, Nagoya City University Graduate School of Medical Sciences, 1 Kawasumi, Mizuho-cho, Mizuho-ku, Nagoya, Aichi 467-8601, Japan

Elucidation of the mechanism of transcriptional silencing of human immunodeficiency virus type 1 (HIV-1) provirus in latently infected cells is crucial to understand the pathophysiology of HIV-1 infection and to develop novel therapies. Here we demonstrate that AP-4 is responsible for the transcriptional repression of HIV-1. We found that AP-4 site within the viral long terminal repeat (LTR) is well conserved in the majority of HIV-1 subtypes and that AP-4 represses HIV-1 gene expression by recruiting histone deacetylase (HDAC) 1 as well as by masking TATA-binding protein to TATA box. AP-4-mediated transcriptional repression was inhibited by an HDAC inhibitor, tricostatin A, and could be exerted even at distant locations from the TATA box. In addition, AP-4 interacted with HDAC1 both *in vivo* and *in vitro*. Moreover, chromatin immunoprecipitation assays have revealed that AP-4 and HDAC1 are present in the HIV-1 LTR promoter in latently infected ACH2 and U1 cells, and they are dissociated from the promoter concomitantly with the association of acetylated histone H3, TBP, and RNA polymerase II upon TNF-α stimulation of HIV-1 replication. Furthermore, when AP-4 is knocked down by siRNA, HIV-1 production was greatly augmented in cells transfected with a full-length HIV-1 clone. These results suggest that AP-4 may be responsible for transcriptional quiescence of latent HIV-1 provirus and give a molecular basis to the reported efficacy of combination therapy of conventional anti-HIV drugs with an HDAC inhibitor in accelerating the clearance of HIV-1 from individuals infected with the virus.

Human immunodeficiency virus type 1 (HIV-1)[2] is a cytopathic retrovirus and the primary etiological agent of acquired immunodeficiency syndrome (AIDS) and related disorders. Among the various steps of viral life cycle, the step of transcription from HIV-1 provirus is conceived to be crucial for viral replication since amplification of the viral genetic information is attainable only through transcription. HIV-1 transcription is directed by the promoter located in the 5′ long terminal repeat (LTR) of the integrated provirus and is controlled by cellular factors that bind to the multiple *cis*-regulatory elements located in the LTR as well as the virally encoded Tat protein (reviewed in Refs. 1 and 2). In cells chronically infected with HIV-1, activation of nuclear factor-κB (NF-κB) by external stimuli such as tumor necrosis factor (TNF)-α and its binding to LTR triggers the initiation of transcription of viral genes including Tat, which results in explosive HIV-1 replication (reviewed in Refs. 3 and 4). However, little is known how transcription from HIV-1 provirus remains silent during the viral latency.

There are multiple mechanisms known to be involved in the negative regulation of HIV transcription including elimination of transcriptional activator TATA-binding protein (TBP) transcriptional factor IID (TFIID) and the initiator protein complex by leader-binding protein (LBP)-1 (5) and YY-1 (6) that recruits histone deacetylase (HDAC) (7, 8), and actions of transcription factors that interact with the negative regulatory element (NRE) located from −340 to −184 of HIV-1 LTR (2, 9). Regarding the action of NRE, the mechanism by which NRE exerts its negative effect on transcription remains unknown because most of the transcription factors that interact with NRE are transcriptional activators. In addition, an *in vitro* study has revealed a potential role of activator protein (AP)-4 in blocking the TBP binding to TATA box (10). However, biological significance of this finding has not been clarified although the sequence comparison has revealed conservation of AP-4 sites in the majority of HIV-1 isolates (Fig. 1*A*) (11–13).

The HIV-1 LTR TATA box is located at −27 to −23 relative to the transcription initiation site (2, 11–14). TFIID interacts with TATA box and is crucial for HIV-1 gene expression (9, 14–16). TFIID contains the 38-kDa TBP as the major component and induces transcriptional initiation by interacting with other general transcription factors and recruiting RNA polymerase II (RNAPII) (17). TBP (TFIID) also serves as the target of DNA-binding factors binding to the *cis*-regulatory elements within HIV-1 LTR in both positive and negative fashions and thus determines its promoter activity (reviewed in Refs. 16, 18, and 19).

AP-4 is a ubiquitously expressed transcription factor of the basic helix-loop-helix leucine-zipper (bHLH-Zip) subgroup of bHLH proteins and binds to the symmetrical DNA sequence 5′-CAGCTG-3′ (20, 21). AP-4 site is found adjacent (−21/−16) to the HIV-1 TATA box (−27/−23) (10). Although AP-4 was initially identified as a cellular protein that binds to the simian virus 40 (SV40) enhancer and activates the viral late gene transcription (21), transcriptional repression by AP-4 was reported in a number of other genes including angiotensinogen (21) and E7 oncoprotein of human papillomavirus type 16 (23). In addition, we recently found that AP-4 negatively regulates transcription of 8-oxo guanine DNA glycosylase 1 (*OGG1*) gene (24). However, because AP-4 sites are not located adjacent to the TATA box in these promoters, the molecular mechanism of its repressive action is yet to be clarified.

In this study we investigated the role of AP-4 in HIV-1 gene expression. Here we show that AP-4 represses HIV-1 transcription by recruiting HDAC1 as well as by masking the TBP to the HIV-1 TATA box. Biological and therapeutic implications are discussed.

* This work was supported by grants-in-aid from the Ministry of Health, Labor and Welfare of Japan, the Ministry of Education, Culture, Sports, Science, and Technology of Japan. The costs of publication of this article were defrayed in part by the payment of page charges. This article must therefore be hereby marked "*advertisement*" in accordance with 18 U.S.C. Section 1734 solely to indicate this fact.

[1] To whom correspondence should be addressed: Dept. of Molecular and Cellular Biology, Nagoya City University Graduate School of Medical Sciences, 1 Kawasumi, Mizuho-cho, Mizuho-ku, Nagoya, Aichi 467-8601, Japan. Tel.: 81-52-853-8204; Fax: 81-52-859-1235; E-mail: tokamoto@med.nagoya-cu.ac.jp.

[2] The abbreviations used are: HIV-1, human immunodeficiency virus type 1; AIDS, acquired immunodeficiency syndrome; LTR, long terminal repeat; TBP, TATA-binding protein; HDAC, histone deacetylase; NRE, negative regulatory element; aa, amino acids; GST, glutathione *S*-transferase; EMSA, electrophoretic mobility shift assay; ChIP, chromatin immunoprecipitation assay; TNF, tumor necrosis factor; TSA, tricostatin A; ELISA, enzyme-linked immunosorbent assay.

EXPERIMENTAL PROCEDURES

Cell Culture—CEM, HL-60, Jurkat, ACH2, and U1 cells were maintained at 37 °C in RPMI 1640 (Sigma) with 10% fetal bovine serum (Sigma), penicillin (100 units/ml), and streptomycin (100 μg/ml). To maintain the latency of the HIV-1 in ACH2 and U1, 20 μM AZT was added in the culture medium and was excluded prior to experiments. Human embryonic kidney 293 cells were grown at 37 °C in Dulbecco's modified Eagle's medium (Sigma) with 10% heat-inactivated fetal bovine serum, penicillin, and streptomycin.

Plasmids—Construction of mammalian expression plasmids pMyc-AP-4, containing the full-length AP-4 cDNA, pCMV-Tat, and pNL4-3 were described previously (24, 25). pCMV-TBP was a generous gift from T. Tamura (Chiba University). To generate pcDNA-AP-4 (full), pcDNA-ΔN100 AP-4 (100–355 aa), pcDNA-ΔN143 AP-4 (143–355 aa), pcDNA-ΔN180 AP-4 (180–355 aa), pcDNA-ΔC179 AP-4 (1–179 aa), and pcDNA-ΔC130 AP-4 (1–130 aa), each containing a FLAG epitope tag in the N terminus and a V5 epitope tag in the C terminus, the various portions of AP-4 cDNA were amplified by PCR using pMyc-AP-4 as a template with 5′ and 3′ oligonucleotide primers. These products were subcloned into pcDNA 3.1 TOPO V5 vector (Invitrogen). Construction of HIV-1 LTR-based luciferase expression plasmid: CD12-luc (containing the HIV-1 LTR U3 and R) was previously described (25). The mutant HIV-1 LTR luciferase reporter constructs lacking AP-4 binding were generated using a QuikChange site-directed mutagenesis kit (Stratagene). The mutant sequences (sense strand) utilized were the following: CD12-luc-m1, GAT CCT GCA TAT AAG tcg cga CTT TTT GCC TGT AC; CD12-luc-m2, GCA TAT AAG CAG CTc CTT TTT GCC TGT AC; CD12-luc-m3, GCA TAT AAG CAG Cgc TTA AGA TAC AGC; CD12-luc-m4, CCT GCA TAT AAG CAG tcG CTT TTT GCC TGT AC (consensus AP-4 binding sites are underlined, and the mutated sequences are in small letters). The mutant HIV-1 LTR-directed reporter constructs, in which the authentic AP-4 site is mutated and an AP-4 site is aberrantly inserted into various positions of the CD12-luc-m2 reporter plasmid, were constructed by PCR using CD12-luc-m2 DNA as a template and site-directed mutagenesis kit with the following mutagenesis oligonucleotide primer pairs: CD12-luc-m2(+55), forward (5′-GCT AGC TAG GGA ACA GCT GCC CAC TGC TTA AG-3′) and reverse (5′-CTT AAG CAG TGG GCA GCT GTT CCC TAG CTA GC-3′); CD12-luc-m2(−79), forward (5′-CTG GGG ACT TTC CAC AGC TGG GGA GGC GTG GCC-3′) and reverse (5′-GGC CAC GCC TCC CCA GCT GTG GAA AGT CCC CAG-3′); CD12-luc-m2(-150), forward (5′-GTG GCC CGA GAG CTC AGC TGG CAT CCG GAG TAC-3′) and reverse (5′-GTA CTC CGG ATG CCA GCT CAG CTC TCG GGC CAC-3′); CD12-luc-m2(−400), forward (5′-GAT CTG TGG ATC TCA GCT GAC CAC ACA CAA GG-3′) and reverse (5′-CCT TGT GTG TGG TCA GCT GAG ATC CAC AGA TC-3′). The mutant pNL4-3 containing mutation in AP-4 binding was generated using a QuikChange II XL site-directed mutagenesis kit (Stratagene) (24) with oligonucleotide primer pairs: forward, 5′-CAT ATA AGC AGC TcC TTT TTG CCT GTA C-3′ and reverse 5′-GTA CAG GCA AAA AGg AGC TGC TTA TAT G-3′ (mutated AP-4 binding sites are underlined and the mutated nucleotides are in lowercase letters). We first constructed the 5′-LTR AP-4 site mutant in the background of pNL4-3 by site-directed mutagenesis and additional AP-4 site mutation in the 3′-LTR was subsequently introduced into this mutant by site-directed mutagenesis. All constructs were confirmed by dideoxynucleotide sequencing using ABI PRISM™ dye terminator cycle sequencing ready kit (PerkinElmer Life Sciences) on an Applied Biosystems 313 automated DNA sequencer.

Recombinant Protein and Purification—pGEX expression vector (Amersham Biosciences) was utilized to express glutathione *S*-transferase (GST) fusion proteins in bacteria. To generate pGEX-AP-4-expressing GST-AP-4, the AP-4 cDNA was amplified by PCR using pMyc-AP-4 as a template with oligonucleotide primer pairs: forward, 5′-CGG GAT CCC GGA GTA TTT CAT GGT GCC CAC TCA G-3′, containing an BamHI site; reverse, 5′-GGA ATT CCT CAG GGA AGC TCC CCG TCC CCC G-3′, containing an EcoRI site. This product was digested with BamHI and EcoRI, and subcloned in-frame into pGEX-5X-3 vector at the BamHI/EcoRI sites. pGEX-AP-4 was transformed in *Escherichia coli* strain DH5 and expression of recombinant GST-AP-4 protein was induced by 0.1 mM isopropyl-1-thio-β-D-galactopyranoside at 25 °C for 6 h. Recombinant GST proteins were purified by affinity chromatography on glutathione-agarose beads as described previously (26).

Electrophoretic Mobility Shift Assay (EMSA)—The experimental procedure was carried out as described previously (24). Purified recombinant TBP and GST-TBP proteins were purchased from Promega and Santa Cruz Biotechnology, respectively. The double-stranded DNA oligonucleotides corresponding to −42/+4 of HIV-1 LTR (CD12) containing the binding sites of TBP and AP-4 and their mutants were synthesized. The wild-type and mutant oligonucleotide sequences (sense strand) were the following: wild-type (5′-CCC TCA GAT CCT GCA TAT AAG CAG CTG CTT TTT GCC TGT A-3′) and mutants (the underlined AP-4 site has been changed to TGACGG (m1), TAGCTC (m2), CAGCGC (m3), and CAGTCG (m4)) (Fig. 2*B*). These oligonucleotides were labeled using the 5′-end-labeling kit (Takara, Otsu, Shiga, Japan) in the presence of [γ-^{32}P]dATP (Amersham Biosciences). DNA binding reactions were performed at 30 °C for 30 min for TBP and room temperature for 20 min for AP-4. Analysis of protein-DNA complexes was performed by electrophoresis in 6% native polyacrylamide gels with 0.5× Tris borate-EDTA buffer at a constant voltage of 125 V at 4 °C, followed by autoradiography. The specificity of DNA binding was assessed by preincubating with purified GST-AP-4, GST-TBP, or control GST proteins with specific antibodies or competitors for 20 min prior to the addition of the probe.

Anti-AP-4 Antibody—Anti-AP-4 antibody was obtained by immunizing rabbits with GST-AP-4 fusion protein as no immunoprecipitable anti-AP-4 antibody was currently available from any commercial source. The immunized rabbit anti-AP-4 sera were affinity-purified by passing through affinity columns, and the lack of immunoreactivity with GST and other *E. coli* components was confirmed.

Immunoprecipitation and Immunoblot Assays—The experimental procedures for immunoprecipitation and immunoblotting were performed as described (24, 27). Briefly, cells were harvested with lysis buffer (25 mM HEPES-NaOH, pH 7.9, 150 mM NaCl, 1.5 mM $MgCl_2$, 0.2 mM EDTA, 0.3% Nonidet P-40, 1 mM dithiothreitol, 0.5 mM phenylmethylsulfonyl fluoride). The lysates were cleared by centrifugation, and the supernatants were incubated with anti-AP-4 antibody overnight at 4 °C. Immune complexes were washed three times with 1 ml of lysis buffer and antibody-bound proteins were dissolved by boiling in 2× Laemmli sample buffer. After centrifugation, the supernatant proteins were separated by SDS-PAGE and transferred to nitrocellulose membrane (Hybond-C, Amersham Biosciences). The membrane was probed with anti-AP-4 antibody, and immunoreactive proteins were visualized by enhanced chemiluminescence (SuperSignal, Pierce). To evaluate the level of AP-4 protein, cells were similarly treated with the lysis buffer, and the cell lysates were analyzed by immunoblotting using anti-AP-4 or V5 antibody (Invitrogen).

Transfection and Luciferase Assay—293 cells cultured in 12-well plates were transfected using Fugene-6 transfection reagent (Roche Applied Science) as described previously (26, 27). CEM and HL60 cells were transiently transfected by electroporation as reported (24). Briefly,

2×10^7 cells/ml were electroporated with 2 μg of CD12-luc together with 2 μg of pCMV-Tat and indicated amounts of Myc-AP-4 in 400 μl of serum-free RPMI using the Electro Cell Manipulator 600 (BTX Electroporation System) apparatus at 260 V/1050 μfarads. For the internal control, we employed pRL-TK, expressing *Renilla* luciferase under the control of the thymidine kinase promoter not containing the AP-4 site. The transfected cells were harvested, and the extracts were subjected to the luciferase assay using the Luciferase Assay System™ (Promega). All the experiments were carried out in triplicates, and the data were presented as the fold increase in luciferase activities (means ± S.D.) relative to the control for three independent transfections.

RNA Interference—The siRNAs with two thymidine residues (dTdT) at the 3′-end of the sequence were synthesized by Takara. The target sequences were as follows: AP-4-1 (5′-GUG CCC UCU UUG CAA CAU U-3′), AP-4-2 (5′-GGU CAU CAA CUC UGU UUC C-3′), and GFP (5′-GGC UAC GUC CAG GAG CGC ACC-3′). Transfection of siRNA was performed using Lipofectamine 2000 (Invitrogen) reagents.

In Vitro Binding Assay—An *in vitro* protein-protein interaction assay was carried out as described previously (26). Briefly, AP-4 and luciferase proteins were labeled with [^{35}S]methionine *in vitro* transcription/translation using the TnT wheat germ extract-coupled system (Promega) according to the manufacturer's protocol. Approximately 20 μg of GST fusion proteins were immobilized on 20 μl of glutathione-Sepharose beads and washed two times with 1 ml of modified HEMNK buffer (20 mM HEPES-KOH, pH 7.5, 100 mM KCl, 12.5 mM $MgCl_2$, 0.2 mM EDTA, 0.3% Nonidet P-40, 1 mM dithiothreitol, 0.5 mM phenylmethylsulfonyl fluoride). After the final wash, 0.6 ml of beads suspension was incubated with radiolabeled proteins for 12 h at 4 °C. The beads were then washed two times with 1 ml of HENMK buffer and two times with HENMK buffer containing 150 mM KCl. Bound radiolabeled proteins were eluted with 30 μl of Laemmli sample buffer, boiled for 3 min, and resolved by 10% SDS-PAGE.

Chromatin Immunoprecipitation (ChIP) Assay—ChIP assay was performed according to the provider's protocol (Upstate Biotechnology) with some modifications as previously described (24). Briefly, cells were cross-linked with 1% formaldehyde for 10 min at room temperature, washed twice with ice-cold phosphate-buffered saline, and lysed for 10 min at 2×10^6 cells in 200 μl of SDS lysis buffer. The cross-linked chromatin was sheared by sonication 13 times for 10 s at one-third of the maximum power of microson XL sonicator (Wakenyaku, Co., LTD., Kyoto, Japan) with 20 s of cooling on ice between each pulse. Cross-linked and released chromatin fractions were precleared with salmon sperm DNA and protein A-agarose beads for 1 h, followed by immunoprecipitation with the desired antibodies overnight at 4 °C. The immunoprecipitates were sequentially washed once with lysis buffer, twice with high salt buffer, twice with low salt buffer, and twice with TE buffer. After the wash, immune complexes were collected with salmon sperm DNA and protein A-agarose beads at room temperature for 1 h and extracted with 1% SDS, 0.1 M $NaHCO_3$. The eluted samples were reverse cross-linked by proteinase K at 45 °C for 1 h and treated with RNase at 37 °C for 1 h. DNA was recovered by phenol/chloroform and chloroform extractions, and ethanol precipitation. Finally, DNA was dissolved in 30 μl of TE buffer and subjected to PCR. The primer sequences used for PCR were the following: HIV-1 LTR (−109 to +79): forward (5′TAC AAG GGA CTT TCC GCT GG-3′) and reverse (5′-TTG AGG CTT AAG CAG TGG G-3′); β-actin promoter (−980 to −915) (as a control): forward (5′-TGC ACT GTG CGG CGA AGC-3′) and reverse (5′-TCG AGC CAT AAA AGG CAA-3′). The number of PCR cycles was as the following: 33 PCR cycles for all the ChIP experiments and 24 PCR cycles for the input samples, in which PCR amplification was obtained under the linear range of AP-4 binding to the HIV-1 LTR DNA. For each reaction, 10% of cross-linked released chromatin was saved and reversed by proteinase K digestion at 45 °C for 1 h followed by DNA extraction, and the recovered DNA was used as input control.

Antiviral Assay and Measurement of Viral p24 Antigen—Antiviral activity of AP-4 was evaluated based on the extent of inhibition of viral antigen expression in the culture supernatants of Jurkat or 293 cells transfected with a full-length HIV-1 molecular clone (pNL4-3) or mutant pNL4-3, in which AP-4 site is mutated. 293 cells were transfected with 0.1 μg of pNL4-3, together with various amounts of plasmids encoding wild-type AP-4 or AP-4 mutants with Fugene-6 transfection reagent. For siRNA studies, 100 nM siRNAs were introduced with 0.1 μg of pNL4-3 using Lipofectamine 2000 reagent. Jurkat cells were transfected by Nucleofector™ kit V for Jurkat cell (Amaxa Biosystems) according to the manufacturer's protocol. Briefly, 3×10^6 cells were mixed with 0.2 μg of wild-type or mutant pNL4-3 together with indicated amounts of FLAG-AP-4 in 100 μl of Nucleofector™ solution V. These samples were transferred into a transfection cuvette and subjected to electroporation using program T-14. The transfected cells were incubated in culture flasks with a complete media for 36 h. Then, cells were incubated for an additional 24 h in the presence or absence of TNF-α (3 ng/ml). The p24 antigen level in the cell culture supernatant was measured by p24 antigen capture ELISA assay using a commercial kit (RETRO-TEK HIV-1 p24 Antigen ELISA kit; Zepto Metrix Corp., Buffalo, NY) as described previously (25).

RESULTS

AP-4 Competes with TBP for Binding to the HIV-1 TATA Element—The HIV-1 TATA is located at nucleotide position from −27 to −23 relative to the transcription initiation site. The consensus AP-4 site, CAGCTG, is located −21 to −16 nucleotides immediately downstream of the TATA box. The AP-4 binding site in the HIV-1 LTR appears to be conserved in the majority of HIV-1 isolates (11–13). As shown in Fig. 1*A*, a majority of HIV-1 clones contain typical AP-4 binding sequence, CAGCTG, whereas it is mutated to CAGCCG in HIV-1 subtypes F1-F2, G, O, and 01-AE.

Because the AP-4 binding site is located close to the TATA box, we first examined the effect of AP-4 on the binding activity of TBP to the TATA box *in vitro*. To address this issue, recombinant AP-4 protein was produced and purified (Fig. 1, *B* and *C*). As shown in Fig. 1*D* (*left panel*), EMSA analysis using a DNA probe (−42/+4) containing both the TATA box and AP-4 site, showed that AP-4 blocked the TBP binding to TATA box in a dose-dependent manner (*lanes 6* and *7*). The control GST proteins did not alter the DNA binding activity of TBP (Fig. 1*D*, *right panel*). These results were consistent with a previous study by Ou *et al.* (10).

Repression of HIV-1 LTR Gene Expression by AP-4—Because AP-4 masks the TBP binding to the HIV-1 TATA box *in vitro*, we examined the effect of AP-4 on transcription from HIV-1 LTR. The luciferase reporter plasmid containing the HIV-LTR (CD12-luc) was cotransfected with an AP-4 expression vector (pMyc-AP-4) into CEM, HL-60, and 293 cell lines. As shown in Fig. 2*A*, the basal transcriptional level from HIV-1 LTR was inhibited by AP-4 in a dose-dependent manner in all the cell lines tested. Upon stimulation of HIV-1 promoter by TNF-α, a physiological inducer of NF-κB, AP-4 could similarly exert its negative effect. In addition, AP-4 also inhibited the Tat-induced HIV-1 gene expression in these cells.

To address whether the inhibitory effect of AP-4 depends on the presence of AP-4 site, we have created HIV-1 LTR mutants where the AP-4 binding site was mutated (Fig. 2*B*). As shown in Fig. 2*C*, EMSA confirmed that these mutants lost AP-4 binding. Although the inhibitory effect of AP-4 on wild-type LTR was clearly observed (Fig. 2*A*), it was abolished when basal, TNF-α-stimulated, and Tat-stimulated gene expression were

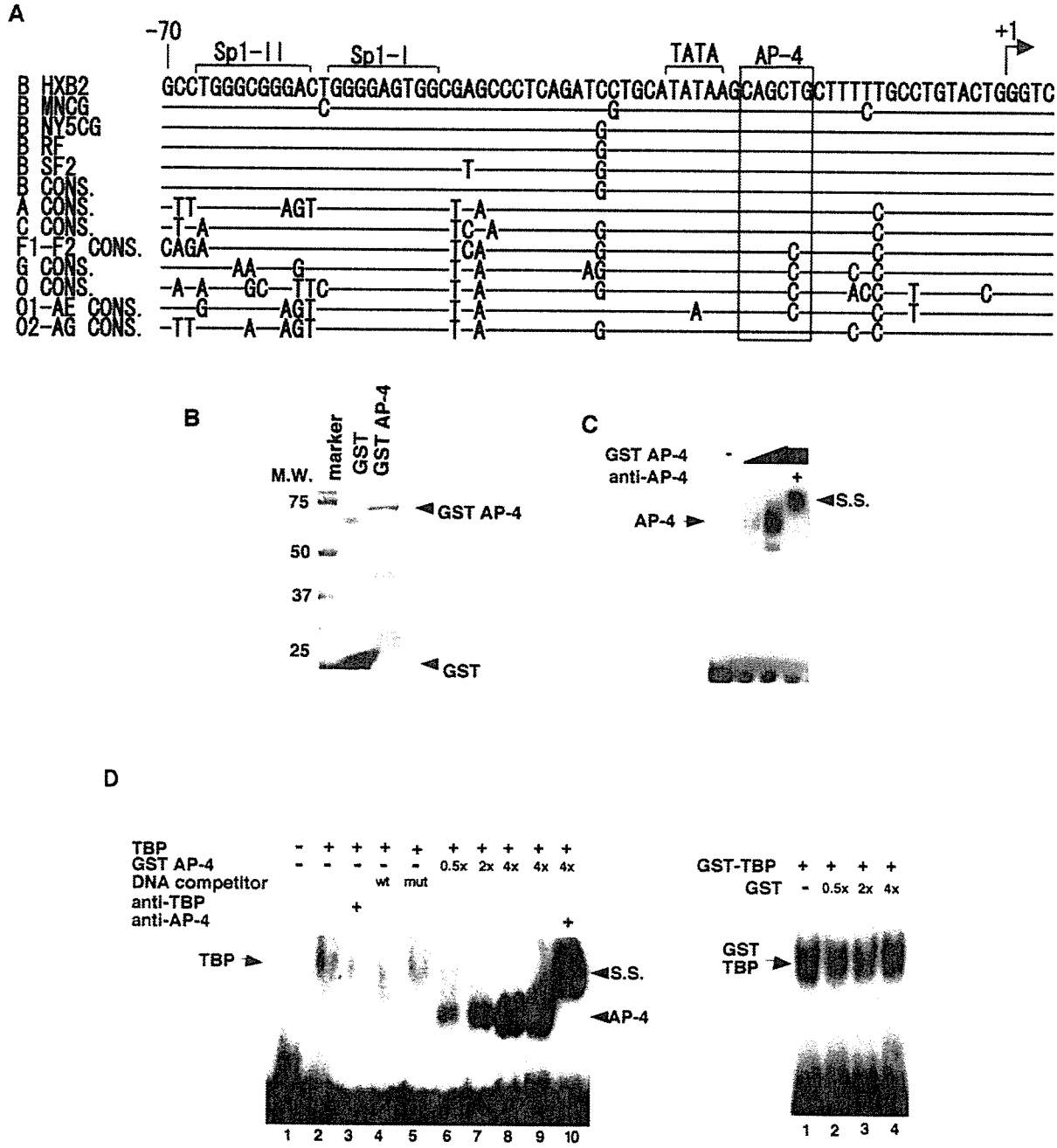

FIGURE 1. **Presence of AP-4 binding site in the vicinity of TATA box of HIV-1 LTR.** *A*, alignment of DNA sequences near the TATA box of various HIV-1 subtypes. The portions of LTR sequences encompassing two Sp1 sites, TATA box, and AP-4 site are shown. AP-4 sites are indicated by a *bracket*. *CONS*, consensus sequences of each HIV-1 subtype. *B*, recombinant GST-AP-4 and GST proteins. The procedures of synthesis and purification are described under "Experimental Procedures." Proteins were resolved by SDS-PAGE and visualized by Coomassie Blue staining. *Arrows* indicate the positions of GST-AP-4 and GST. *C*, DNA binding activity of recombinant GST-AP-4. The DNA binding activity of purified recombinant AP-4 protein was analyzed by EMSA with the ^{32}P-labeled double-stranded oligonucleotide probe containing the TATA box and AP-4 site. To verify the AP-4 and DNA complex, the reaction mixtures were incubated with AP-4 antibody. *D*, effect of AP-4 on the DNA binding activity of TBP. The TBP-DNA binding was analyzed by EMSA using the same probe as *C*. TBP was preincubated with various amounts of either GST-AP-4 at the molar ratios indicated (*left panel*). To verify the TBP-DNA and AP-4-DNA complexes, the reaction mixtures were incubated with the TBP and AP-4 antibodies, respectively. For the cold DNA competition experiment, unlabeled double-stranded competitor oligonucleotides (containing wild-type (*wt*) or mutated (*mut*) TATA sequences) were added to the reaction mixtures at 30-fold excess relative to the DNA probe. To confirm that the GST moiety does not affect the TBP-DNA binding, GST-TBP was preincubated with GST prior to the DNA binding reaction (*right panel*). Experiments were carried out at least three times, and reproducible results were obtained. The representative results are shown. Positions of specific DNA-protein complex and supershifted complex (*S.S.*) are indicated by *arrows*.

assessed with mutant HIV-1 LTR reporter constructs (Fig. 2*D*). To further address whether the inhibitory effect of AP-4 depends on the presence of AP-4 site, we repeated similar experiments using other luciferase reporter plasmids including 5× κB-TATA-luc and 4× CRE-TATA-luc (26), in which no AP-4 site is present. AP-4 did not inhibit gene expression from 5× κB-TATA-luc nor 4× CRE-TATA-luc (data not shown). These results demonstrated for the first time that AP-4 exhibits repressive action on HIV-1 gene expression in cultured cells *in vivo*.

Overexpression of TBP Overcomes the Inhibitory Effect of AP-4—To confirm that the repressive effect of AP-4 is through masking the TBP binding to the HIV-1 TATA box, we examined the effect of TBP overexpression on the action of AP-4. As shown in Fig. 3*A*, the inhibitory effect of AP-4 on basal gene expression was abrogated by TBP overexpression in a dose-dependent manner. Similarly, AP-4-mediated repression of the TNF-α-stimulated HIV-1 gene expression was abolished by TBP overexpression (Fig. 3*B*).

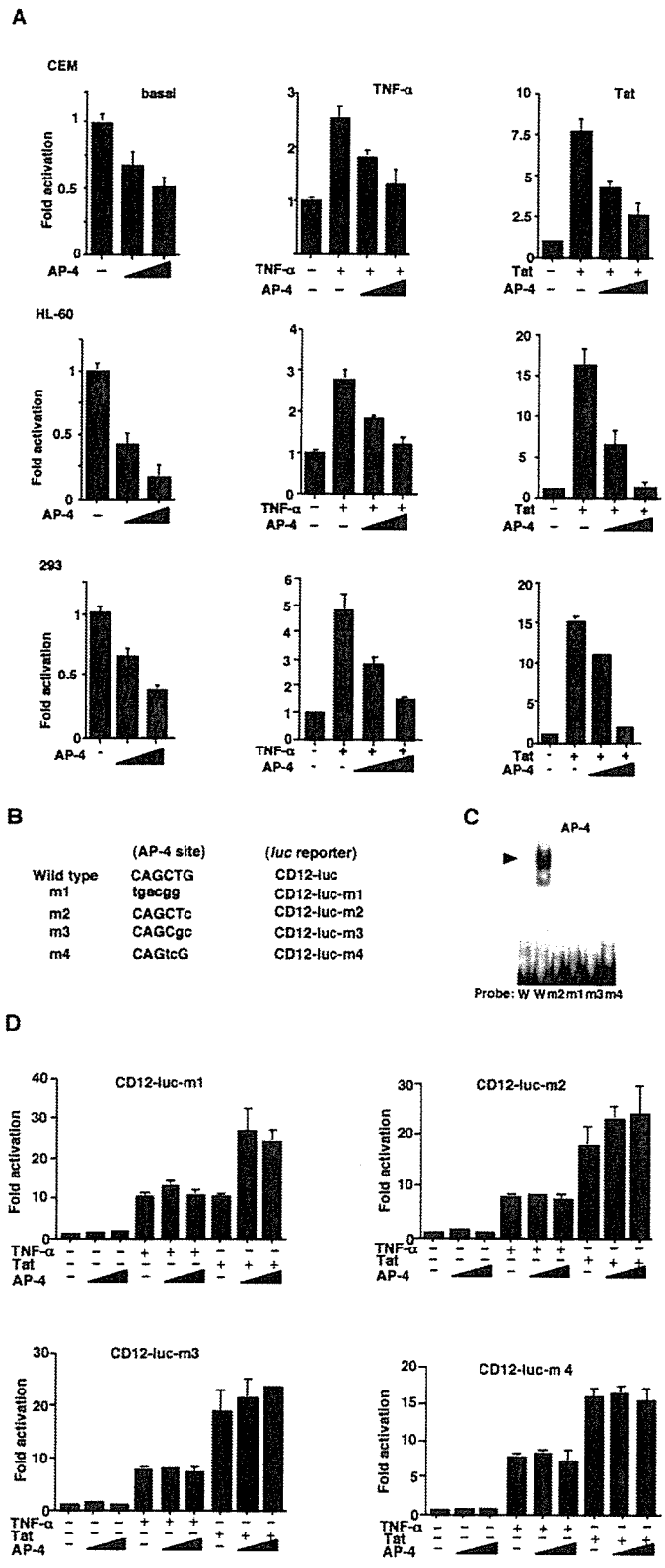

FIGURE 2. **Repression of HIV-1 gene expression by AP-4.** *A*, AP-4-mediated repression of HIV-1 gene expression. AP-4 expression plasmid pMyc-AP-4 was cotransfected with CD12-luc reporter construct, expressing luciferase gene under the control of HIV-1 LTR, into CEM, HL-60 or 293 cells. Extents of HIV-1 gene expression and the effects of AP-4 were evaluated at the basal level (*left panels*), upon TNF-α stimulation (*middle panels*), or upon Tat-mediated transactivation by cotransfecting pCMV-Tat at 2 and 0.1 mg per transfection for CEM/HL60 and 293 cells, respectively (*right panels*). pMyc-AP-4 were cotransfected at 2 and 12 μg for CEM and HL60 cells, and 0.1 and 0.4 μg for 293 cells per transfection. In the TNF-α experiments, cells were stimulated with TNF-α (3 ng/ml) after 24 h of transfection and incubated for additional 24 h. The cells were harvested and the luciferase activity was measured. Each value shown is the fold increase in the luciferase activity (means ± S.D.) relative to the control transfection for three independent experiments. Luciferase activity was measured as above. The values shown are the means ± S.D. for three independent experiments. *B*, the sequences of wild-type and AP-4 binding site mutants. These mutant sequences (m1 to m4) were used in EMSA and luciferase assays by replacing the authentic AP-4 site within CD12-luc (named as CD12-luc-m1 to CD12-luc-m4). *C*, lack of AP-4 DNA binding to mutant AP-4 sequences. The DNA binding activities of purified recombinant AP-4 protein was analyzed by EMSA with the wild-type and mutant AP-4 probes. *Arrowheads* indicate the positions of specific DNA-protein complex. *D*, effects of AP-4 binding site mutation on the AP-4-mediated repression. 293 cells were transfected with mutant CD12-luc containing mutations in the AP-4-site together with various amounts of pMyc-AP-4 (0.1 and 0.4 μg per transfection) with or without stimulation of TNF-α (3 ng/ml) or cotransfection of pCMV-Tat. The luciferase activity was measured as in *A*.

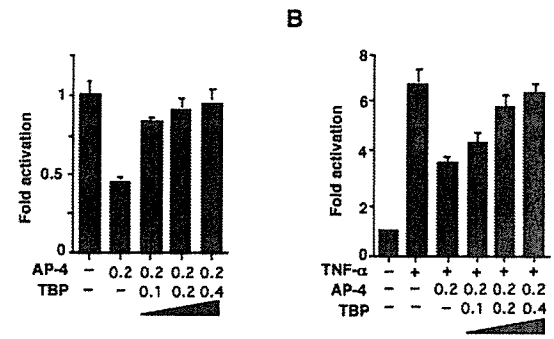

FIGURE 3. **Overexpression of TBP overcomes the repressive effect of AP-4 on HIV-1.** 293 cells were transfected with CD12-luc in combination with pMyc-AP-4 and pCMV-TBP expressing AP-4 and TBP, respectively. After 24 h, cells were untreated (*A*) or treated (*B*) with TNF-α (3 ng/ml) and incubated for additional 24 h. Cells were harvested, and the luciferase activity was measured as described in the legend to Fig. 2.

The Effect of AP-4 Knock-down—To examine the effect of endogenous AP-4, we adopted siRNA technique to specifically knock-down AP-4 mRNA and examined the HIV-1 gene expression when the endogenous AP-4 was depleted. Transduction of AP-4 siRNA caused the depletion of AP-4 protein (Fig. 4*A*), which resulted in significant increase in the basal transcriptional level from HIV-1 LTR (8.2-fold as compared with control siRNA) (Fig. 4*B*). In addition, TNF-α-stimulated LTR gene expression was greatly elevated by AP-4 depletion (5.7-fold). These results indicate that endogenous AP-4 acts as a negative regulator of HIV-1 gene expression.

The DNA Binding Activity of AP-4 Is Essential for the Repression of HIV-1 Gene Expression—AP-4 contains three functional domains, a basic HLH (bHLH) motif (48–99 aa) and two distinct leucine repeat elements, leucine repeat (LR) 1 (99–120 aa) and LR2 (151–179 aa) (Fig. 5*A*). A previous study (20) showed that the HLH motif and an adjacent basic domain are necessary and sufficient to direct sequence-specific DNA binding to its target DNA. Unlike other HLH proteins, AP-4 contains two additional protein dimerization motifs LR1 and LR2. Although both LRs contribute to the formation of AP-4 homodimers, AP-4 requires LR2 to form a stable homodimer (20). The C-terminal half of AP-4 contains a Gln/Pro-rich domain and an acidic region.

To investigate the role of functional domains of AP-4 in down-regulating HIV-1 gene expression, we examined the effects of deletion mutants of AP-4 (shown in Fig. 5*A*). Deletion of the N-terminal regions (ΔN100, ΔN143, and ΔN180) of AP-4 abolished the repressive action on both basal and TNF-α-stimulated HIV-1 expression (Fig. 5*B*). In contrast, deletion of the C-terminal region of AP-4 (ΔC179, retaining the bHLH and two LR domains) repressed HIV-1 gene expression similarly to the full-length AP-4. These results indicate that bHLH domain is indispensable for the repression of HIV-1 gene expression. Because inhibitory effect of ΔC130 (excluding LR2 domain from the ΔC179) was weaker than ΔC179, AP-4 dimerization is important for its effect through stabilization of AP-4 homodimer (20).

Effect of the Location of AP-4 Site Within HIV-1 LTR on the Repressive Effect of AP-4—To further examine whether the repressive effect of AP-4 depends on its location relative to the TATA box within HIV-1 LTR, we created mutant HIV-1 LTR reporter constructs in which AP-4 binding sites were inserted into various positions of the HIV-1 LTR. Thus, AP-4 binding site were inserted at nucleotide positions −400, −15, −79, and +55 (Fig. 6*A*) within HIV-1 LTR into CD12-luc-m2 in which the authentic AP-4 site was mutated. Basal promoter activities of these promoter constructs were not significantly changed as compared with the original construct (data not shown). As shown in Fig. 6*B*, even when AP-4 sites were distantly located from TATA box, AP-4 could still exert repressive action irrespective of the stimulation by TNF-α. The greatest repressive effect of AP-4 was observed with CD12-luc-m2(−79) although it was less than that with the wild-type promoter. Other AP-4 site mutants exhibited less susceptibility to AP-4-mediated transcriptional repression. These findings indicate that AP-4 could repress HIV-1 transcription even from the distant locations from TATA box although the maximal repressive effect of AP-4 was observed when AP-4 was located in close proximity to the TATA box.

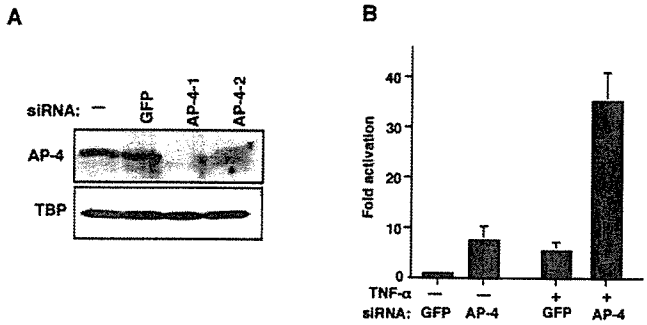

FIGURE 4. **Effect of AP-4 knock-down.** *A*, confirmation of the siRNA-mediated knock-down of AP-4. 293 cells were transfected with 100 nM siRNAs directed against various portions of AP-4 or GFP (control) mRNAs. After 36 h of transfection, cells were lysed, and AP-4 and TBP (control) protein levels were assessed by immunoblotting using specific antibodies. The blot was stripped and reprobed with anti-α-tubulin antibody. *B*, augmentation of HIV-1 gene expression by AP-4 depletion. 293 cells were transfected with CD12-luc together with AP-4 siRNA-1 or its control. After 24 h of transfection, cells were untreated or treated with 3 ng/ml of TNF-α and incubated for an additional 24 h. Cells were harvested, and the luciferase activity was measured as described in the legend to Fig. 2.

Interaction of HDAC with AP-4—Cumulative evidence has demonstrated that chromatin modification by HDAC complex plays a significant role in transcriptional repression (reviewed in Refs. 10 and 48) and many transcriptional repressors, such as YY-1 (8), silencing mediator of retinoic acid and thyroid hormone receptor (28), nuclear receptor corepressor (29), and special AT-rich sequence-binding protein 1 (30) have been shown to tether HDACs to the promoter. Because AP-4 could still exert repressive action even when AP-4 sites were distantly located from TATA box (Fig. 6*B*), we examined whether HDAC was involved in the HIV-1 gene repression by AP-4. To address this possibility we first examined whether AP-4

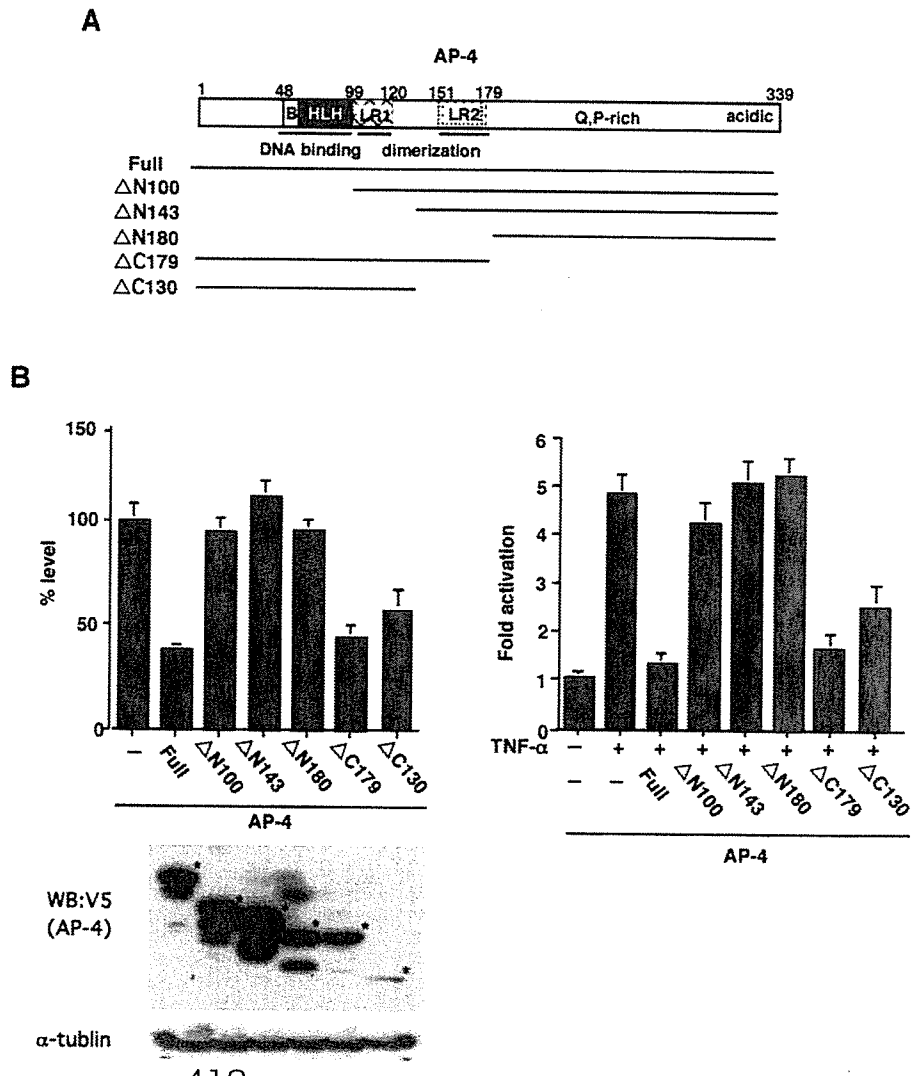

FIGURE 5. **Effects of AP-4 deletion mutants on the HIV-1 gene expression.** *A*, schematic representation of the AP-4 protein and constructs of AP-4 mutants. *Hatched box*, conserved basic stretch; *closed box*, HLH motif; *LR1*, first leucine repeat; *LR2*, second leucine repeat. The amino acid positions of AP-4 are marked on the *top*. *B*, effect of AP-4 mutants on HIV-1 gene expression. Effect of AP-4 was evaluated at the basal level (*left panel*) and upon stimulation with TNF-α (3 ng/ml) (*right panel*). 293 cells were transfected with CD12-luc together with the plasmid expression of wild-type or mutant AP-4. Luciferase assays were performed as described in the legend to Fig. 2. The expression level of each protein was assessed by immunoblotting of cell lysates with anti-V5 antibodies (detecting AP-4 and its mutants). *Asterisks* indicate the positions of specific bands of AP-4 proteins. The low protein level of AP-4 mutant ΔC130, lacking the LR2 domain responsible for protein homodimerization, is considered because of destabilization of the protein.

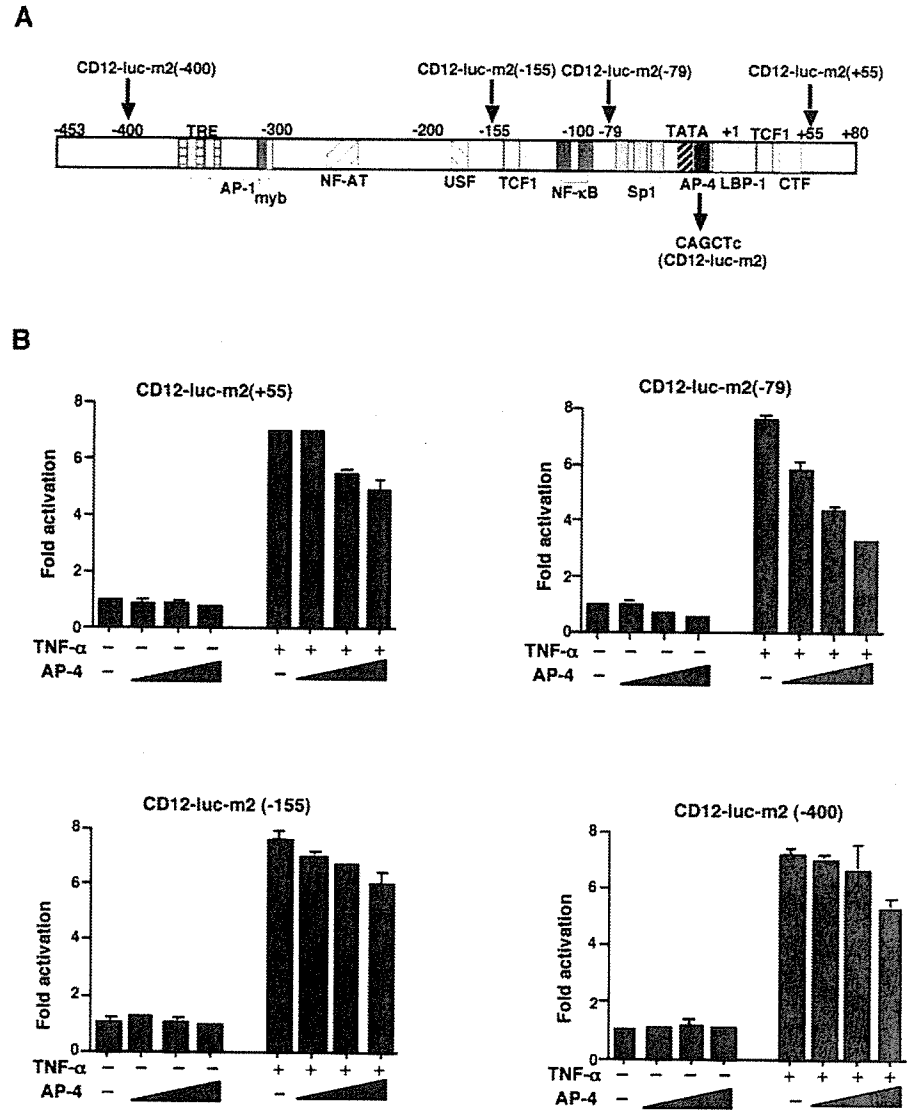

FIGURE 6. **Effects of AP-4 site location on AP-4-mediated repression of HIV-1.** *A*, schematic map of the U3 and R regions of the HIV-1 LTR and positions of aberrant AP-4 sites in mutant constructs. AP-4 site is inserted into various locations (nucleotide positions: −400, −15, −79, and +55) within CD12-luc-m2 (Fig. 2*B*), in which the authentic AP-4 site is abolished. *B*, effect of the AP-4 site on susceptibility to AP-4-mediated repression. 293 cells were transfected with reporter constructs and various amounts of pMyc-AP-4 (0.05, 0.2, and 0.4 μg per transfection). After 24 h, cells were untreated (*left side of each panel*) or treated (*right side*) with TNF-α (3 ng/ml) and incubated for an additional 24 h. The luciferase activity was measured as described in the legend to Fig. 2.

interacts with HDACs in culture cells. In Fig. 7, 293 cells were transfected with FLAG- or Myc- (used as a negative control for immunoprecipitation) tagged AP-4 expression plasmids, and cell lysates were subjected to immunoprecipitation with anti-FLAG antibody. Immune complexes were collected and subjected to SDS-PAGE followed by immunoblotting for detection of the class I HDACs using antibodies to HDAC1, 2, and 3. As shown in Fig. 7*A*, AP-4 interacted with HDAC1, and to a much lesser extent HDAC2, but not detectably with HDAC3. In Fig. 7*B*, similar experiments with untransfected cells showed the interaction of endogenous AP-4 with endogenous HDAC1. The interaction of AP-4 with HDAC2 was observed but much less than that with HDAC1. No interaction between AP-4 and HDAC3 was observed (data not shown). To examine whether AP-4 directly binds to HDAC1, we performed *in vitro* protein-protein interaction assay using GST-AP-4 fusion protein, radiolabeled HDAC1, and luciferase (as a control). The radiolabeled HDAC1 directly bound GST-AP-4 but not GST and no binding was observed between GST-AP-4 and luciferase (Fig. 7*C*). These results demonstrated that AP-4 directly interacts with HDAC1. To further confirm the involvement of HDACs in transcriptional repression of HIV-1 by AP-4, trichostatin A (TSA), a specific inhibitor of HDACs, was added to the cells transfected with AP-4, and the luciferase assay was performed. As shown in Fig. 7*D*, TSA abrogated the repressive effect of AP-4 on HIV-1 gene expression in a dose-dependent manner. These findings suggest that HDACs are involved in the AP-4-mediated repression of HIV-1 gene expression.

ChIP Assays Detecting AP-4 and HDAC1 on HIV-1 LTR—Together with the results demonstrated above, it was suggested that AP-4-mediated HDAC recruitment to and elimination of TBP (TFIID) from the HIV-1 promoter might play a role in the cellular maintenance of HIV-1 latency. We thus examined the presence of AP-4 and HDAC1 on the HIV-1 promoter in latently infected cells, ACH2 (T-cell line latently infected with HIV-1) and U1 (promyelocytic cell line latently infected with HIV-1) (31). As shown in Fig. 8*A*, the newly raised anti-AP-4 antibody could specifically precipitate AP-4. Although the nature and/or the extent of chromatin formation on transiently transfected DNA templates likely differ from that of chromosomal genes, previous reports of ChIP assays using plasmids containing HIV-1 LTR have validated ChIP studies in transiently transfected cells (32–35). In Fig. 8*B*, 293 cells were transiently transfected with CD12-luc or its mutant CD12-luc-m2 followed by ChIP analysis using the anti-AP-4 antibody. We amplified the HIV-1 LTR DNA fragment (−109/+79) containing binding sites for NF-κB, Sp1, TBP, AP-4, LBP-1 (YY-1), TCF1, and CTF (Fig. 6*A*) in the AP-4 and HDAC1 immune complexes. We were able to detect the binding of both AP-4 and HDAC1 to the HIV-1 promoter by ChIP assay in 293 cells transfected with CD12-luc (Fig. 8*B*). The binding

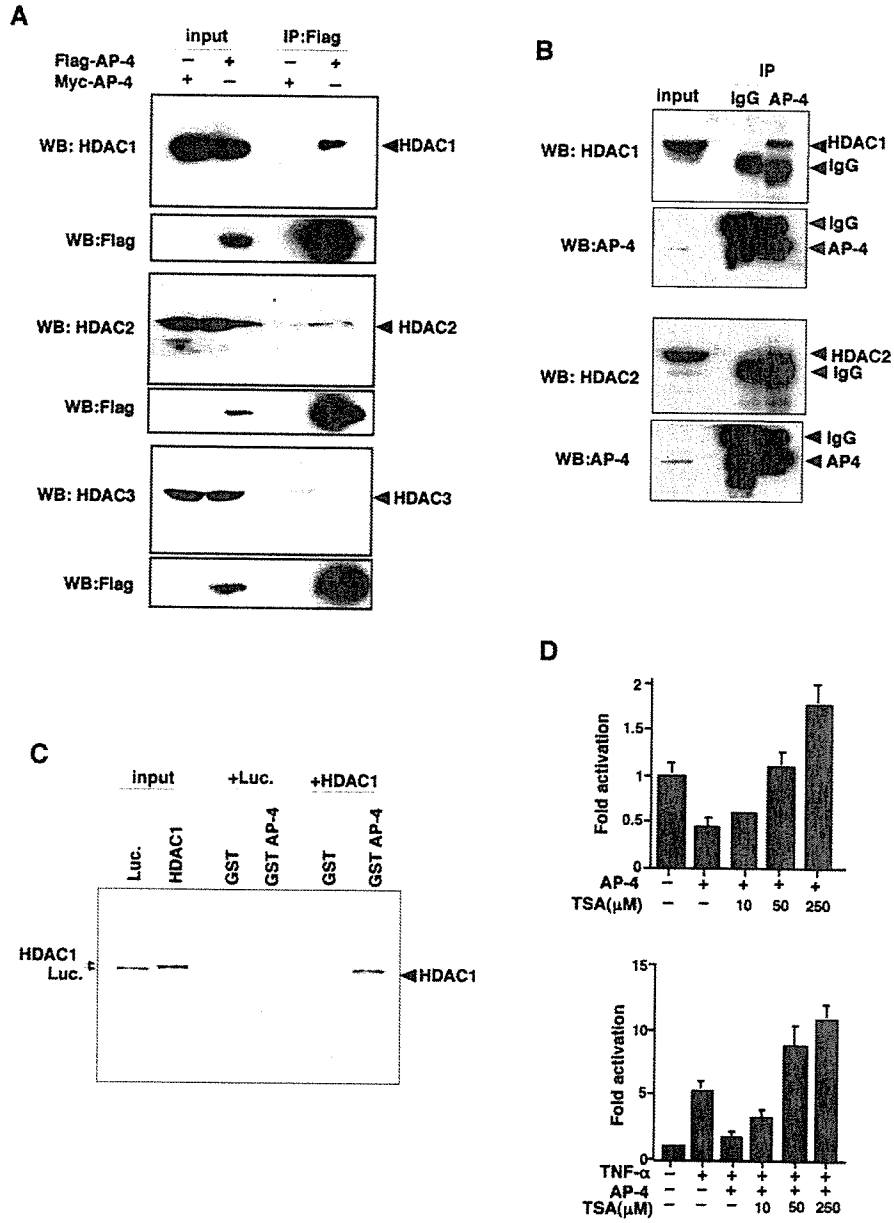

FIGURE 7. **Interaction of HDAC with AP-4.** *A*, interaction between AP-4 and HDAC proteins *in vivo*. 293 cells were transfected with FLAG- (pFLAG-AP-4) or Myc-tagged (pMyc-AP-4) AP-4 expression plasmids. After 48 h of transfection, the cell lysates were prepared, immunoprecipitated with anti-FLAG antibody, and subsequently separated on SDS-PAGE followed by immunoblotting with anti-HDAC antibodies. One-tenth of each protein lysate was loaded as input control. *B*, endogenous AP-4 interacts with HDACs. 293 cell lysates were immunoprecipitated with anti-AP-4 antibody, and the immune complex was analyzed by immunoblotting with anti-HDAC antibodies. *C*, AP-4 binds to HDAC1 *in vitro*. HDAC1 and luciferase (negative control) proteins were synthesized and labeled with [^{35}S]methionine *in vitro*. These radiolabeled HDAC1 and luciferase proteins were incubated with GST-AP-4 or GST (control) immobilized on glutathione-Sepharose beads. After incubation and further washing, the complexes were resolved by SDS-PAGE and subjected to autoradiography. *D*, effect of TSA on the repressive activity of AP-4. 293 cells were transfected with CD12-luc together with pMyc-AP-4. After 24 h of transfection, cells were untreated (*upper panel*) or treated (*lower panel*) with TNF-α (3 ng/ml), incubated for additional 24 h, and various amounts of TSA were added to the culture. After 8 h of additional incubation, cell lysates were prepared, and the luciferase activity was measured as described in the legend to Fig. 2.

with AP-4 or HDAC1 was detectably reduced when CD12-luc-m2, in which AP-4 site was mutated, was transfected. The trace amount of HDAC1 recruitment was detected even with the mutant, presumably due to the presence of binding region (from −10 to +27) of LBP-1 and YY-1, known to recruit HDAC1 (8).

In Fig. 8*C*, ChIP assays were similarly performed with ACH2 and U1 cells using antibodies to AP-4, HDAC1, acetylated histone H3 (Ac-H3), TBP, and RNAPII. AP-4 and HDAC1, but only traceable amounts of TBP (TFIID) or RNAP II, were detected on the HIV-1 promoter when these cells maintained the latency (without any stimulation). However, when ACH2 and U1 cells were treated with TNF-α to stimulate HIV-1 replication, AP-4 and HDAC1 were readily dissociated from the HIV-1 promoter, and TBP and RNAPII became clearly detectable on the HIV-1 promoter over time (Fig. 8*C*). Moreover, the disappearance of AP-4 from the HIV-1 LTR correlated with dissociation of HDAC1 and appearance of the acetylated form of histone H3 (Ac-H3). These results, together with the findings described above, suggest that AP-4 acts as a negative regulator of HIV-1 gene expression by recruitment of HDAC1 as well as by preventing the TBP (TFIID) binding to the TATA box in latently infected cells.

Repression of HIV-1 Production by AP-4—To assess the biological relevance of the repressive action of AP-4, we examined the effect of AP-4 on HIV-1 production. 293 cells were transfected with a replication-competent full-length HIV-1 clone (pNL4-3) together with various amounts of AP-4-expression plasmid pFLAG-AP-4, and virus production was evaluated by measuring HIV-1 p24 antigen levels in the culture supernatant. In Fig. 9*A*, transduction of AP-4 resulted in dose-dependent decrease in the HIV-1 p24 level by 3.7-fold (Fig. 9*A*, *left panel*). Inhibition of viral protein synthesis was also observed in these cells when AP-4 was overexpressed (Fig. 9*A*, *right panel*). In Fig. 9*B*, the effect of AP-4 on the TNF-α-stimulated HIV-1 production was examined. When pNL4-3 was transfected and cells were subsequently stimulated with TNF-α, 7.4-fold increase of HIV-1 production was observed (Fig. 9*B*, *right panel*). When AP-4 was overexpressed, a dramatic inhibition of HIV-1 production was observed in a dose-dependent manner, almost to the basal unstimulated level (Fig. 9*B*). In Fig. 9*C*, effects of AP-4 mutants were examined. Although an AP-4 mutant ΔC179, retaining the AP-4 DNA binding and dimerization domains, could suppress HIV-1 production as well as wild-type AP-4, another mutant ΔN143, lacking these two functional domains, showed no suppressive effect on the HIV-1 pro-